Shape optimization in acoustic–structure interaction

Philipp Kliewe
Institute of Mathematics, TU Berlin, Berlin, Germany
Antoine Laurain
Department of Applied Mathematics, Institute of Mathematics and Statistics, University of São Paulo, São Paulo, Brazil, and
Kersten Schmidt
Department of Mathematics, TU Darmstadt, Darmstadt, Germany

Received 5 July 2021
Revised 9 September 2021
Accepted 10 September 2021

Abstract

Purpose – Motivated by the acoustics of motor vehicles, a coupled fluid–solid system is considered. The air pressure is modeled by the Helmholtz equation, and the structure displacement is described by elastodynamic equations. The acoustic–structure interaction is modeled by coupling conditions on the common interface. First, the existence and uniqueness of solutions are investigated, and then, after recalling fundamental notions of shape optimization, the tensor form of the distributed shape derivative is obtained for the coupled problem. It is then applied to the minimization of the sound pressure by variation of the structure shape through the positioning of beads.

Design/methodology/approach – The existence and uniqueness of solutions up to eigenfrequencies are shown by the Fredholm–Riesz–Schauder theory using a novel decomposition into an isomorphism and a compact operator. For the design optimization, the distributed shape derivative is obtained using the averaged adjoint method. It is then used in a closed 3D optimization process of the position of a bead for noise reduction. In this process, the C++ library concepts are used to solve the differential equations on hexahedral meshes with the finite element method of higher order.

Findings – The existence and uniqueness of solutions have been shown for the case without absorption, where the given proof allows for extension to the case with absorption in the domain or via boundary conditions. The theoretical results show that the averaged adjoint can be applied to compute distributed shape derivatives in the context of acoustic–structure interaction. The numerical results show that the distributed shape derivative can be used to reduce the sound pressure at a chosen frequency via rigid motions of a nonsmooth shape.

Originality/value – The proof of shape differentiability and the calculation of the distributed shape derivative in tensor form allows to consider nonsmooth shapes for the optimization, which is particularly relevant for the optimal placement of beads or stampings in a structural-acoustic system.

Keywords Acoustic–structure interaction, Bead optimization, Shape optimization, Distributed shape derivative

Paper type Research paper

1. Introduction

Acoustic–structure interaction is an emerging field in mathematical modeling and in the industry, with important applications in reducing the noise emitted by vehicles, constructions

JEL Classification — 65N30, 35J25

The second and third authors acknowledge financial support from the DFG Research Center Matheon "Mathematics for key technologies" in Berlin, through Project C37 "Shape/Topology optimization methods for inverse problems" and Project D26 "Asymptotic analysis of the wave-propagation in realistic photonic crystal wave-guides", respectively. The second author also acknowledges financial support from the Brazilian National Council for Scientific and Technological Development (Conselho Nacional de Desenvolvimento Científico e Tecnológico–CNPq) through the process: 408175/2018–4 "Otimização de forma não suave e controle de problemas de fronteira livre" and through the program "Bolsa de Produtividade em Pesquisa–PQ 2018", process: 304258/2018–0.

Engineering Computations

0264-4401
DOI 10.1108/EC-07-2021-0379

and machines in general. In particular in the automotive industry, there is a considerable interest to optimize and tailor the sound amplitudes within cars by changing the shape of parts of the elastic structure. For examples of structural optimization with acoustic applications in the engineering community, we refer to Marburg (2002), Marburg *et al.* (2016) and the references therein. The existence and uniqueness for the acoustic–structure interaction problem were proved first for unbounded (fluid) domains in Barucq *et al.* (2014) based on the Fredholm theory and in bounded domains in Stammberger and Voss (2014) based on the theory of self-adjoint operators, where it is restricted to the case without absorption. We present an alternative proof that simplifies significantly the one given in Barucq *et al.* (2014) and is extendable to the case of absorption in the domain or through Robin boundary conditions.

With the development of computational power in the last decades, numerical methods have become an essential approach for optimizing designs in acoustic–structure interactions. Various approaches to model geometry optimization in the mathematical and engineering communities have been explored. In Antil *et al.* (2017), an optimal control approach is used for shape optimization of shell structure acoustics. Topology optimization approaches such as the Solid Isotropic Material with Penalisation (SIMP) method have been successfully used to solve optimal design problems for acoustic–structure interactions; see for instance (Yoon *et al.*, 2006, 2007; Luo and Gea, 2003; Vicente *et al.*, 2015; Du and Olhoff, 2007, 2010; Akl *et al.*, 2009) and the recent review (Dilgen *et al.*, 2019). However, the lack of an explicit representation of the interface in topology optimization methods may create difficulties when the structural–acoustic interface needs to be optimized, due to the transmission conditions at the interface. The level set method (Osher and Sethian, 1988) allows to have a sharp representation of the interface and has been used successfully in structural optimization; see Laurain (2018), Allaire *et al.* (2004), Wang *et al.* (2003), van Dijk *et al.* (2013). Recently, the level set method has been extended to the coupled acoustic-structural system in Shu *et al.* (2014). In the present paper, we also consider a sharp representation of the interfaces, but we do not use the level set framework as we consider fixed shapes and rigid displacements in the numerics.

The optimization problem is often posed in a discrete setting with a certain number of parameters or degrees of freedom, which corresponds to the approach "first discretize–then optimize." Here, we consider first the optimization problem in the continuous setting, and afterward we discretize the problem using finite elements. This means that the sensitivity of our cost functional with respect to shape perturbations is obtained in a function space framework, using the geometric flow of a reference shape by a vector field. This yields the so-called *shape derivative* of the cost functional; see Delfour and Zolésio (2011), Sokolowski and Zolesio (1992), Henrot and Pierre (2018) for an introduction to this concept. We perform the analysis in the general case of free-form perturbations of the shape, and for the numerical results, we specialize to a specific type of shape perturbations.

Shape optimization algorithms are usually based on the fact that the shape derivative may often be written as a boundary integral, the so-called *boundary expression* of the shape derivative. Using this property, one can compute a descent direction for the cost functional in the form of a boundary vector field. After extending this vector field to a neighborhood of the boundary, it can be used to evolve the domain using a numerical method such as the level set method; see Allaire *et al.* (2004), Fulmański *et al.* (2007, 2008), Hintermüller and Laurain (2009), Wang *et al.* (2003) for examples of this approach.

Alternatively, the shape derivative can also be written as a domain integral, called *distributed*, *volumetric* or *domain expression* of the shape derivative; see Berggren (2010), Hiptmair *et al.* (2015), Laurain and Sturm (2016), Laurain (2020). The distributed expression is well-known, see for instance (Delfour *et al.*, 1985, 1997), but has been usually considered as a mere intermediate step toward the calculation of the boundary expression of the shape derivative. Recently, numerical applications of the distributed shape derivative have

witnessed a surge of interest, see Beretta *et al.* (2017), Eigel and Sturm (2018), Etling and Herzog (2018), Hintermüller *et al.* (2015), Novotny and Sokołowski (2013), Sturm *et al.* (2016), Schmidt (2018), Schulz *et al.* (2016), Giacomini *et al.* (2017), which has been fueled by new theoretical developments. In Berggren (2010), it was shown that the discretization and the shape differentiation processes commute for the distributed expression but not for the boundary expression, meaning that the discretized boundary expression does not generally yield the same expression as the shape derivative computed in the discrete setting. In Hiptmair *et al.* (2015), the authors conclude that distributed shape derivatives often provide better numerical accuracy than boundary representations in a finite element setting. It was also observed that the distributed expression is easier to implement numerically than the boundary expression; see Allaire *et al.* (2014), Laurain (2018), Laurain and Sturm (2016). In Laurain and Sturm (2016), Laurain (2020), properties of the tensor form of distributed shape derivatives were studied. It was shown that the tensor form is convenient for numerical implementation and for the calculation of the corresponding boundary expression. It actually plays an important role in continuum mechanics, with the energy-momentum tensor introduced by Eshelby; see Eshelby (1975), Novotny and Sokołowski (2013).

In this paper, we compute the distributed shape derivative of the cost functional using a Lagrangian method. Such methods are often used in shape optimization, they are convenient for efficiently calculating the shape derivative of the cost functional and the adjoint state; see Céa (1986), Delfour and Zolésio (2011), Pantz (2005), Laurain *et al.* (2020). Here, we use the averaged adjoint method, a Lagrangian-type method introduced in Sturm (2015) that requires minimal hypotheses and naturally provides the distributed shape derivative; see Laurain and Sturm (2016), Gangl *et al.* (2015), Laurain (2018) for applications. To the best of our knowledge, this is the first contribution based on the distributed shape derivative and its tensor form for shape optimization of a structural-acoustic system.

The paper is organized as follows. In Section 2, we define the geometry and the governing equations for the acoustic–structure interaction problem. In Section 3, existence and uniqueness for the acoustic-structural system is proved. In Section 4 the shape sensitivity framework is described and the distributed shape derivative of the cost functional is computed in tensor form. Moreover, for the optimal placement of a bead for noise reduction, search directions are derived from distributed shape derivative for which numerical results, using a finite element discretization of higher order on hexahedral meshes using the C++ library concepts (Frauenfelder and Lage, 2002), are shown and discussed.

2. The model problem

We consider the problem of time-harmonic acoustic–structure interaction in the two open, Lipschitz and piecewise C^1 domains $\Omega_F, \Omega_S \subseteq \mathbb{R}^3$ (see Figure 1), which do not intersect, that is,

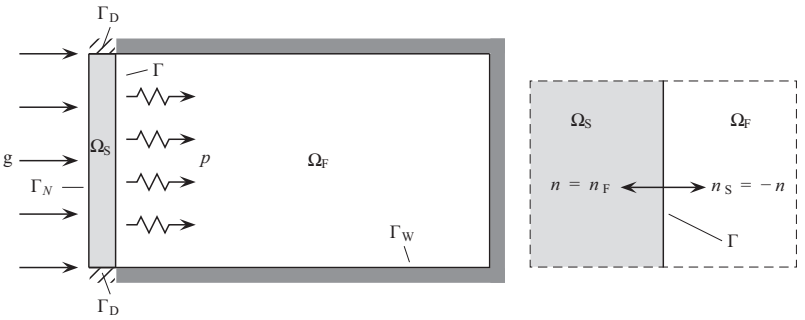

Figure 1.
The geometry of the acoustic–structure interaction problem (*left*) and the convention on the normal vector on the interface between solid and fluid (*right*)

$\Omega_F \cap \Omega_S = \varnothing$. By piecewise C^1, we mean that the domain is of class C^1, except at a finite set of connecting boundary points. The elastic structure represented by Ω_S and the fluid, for example, air, corresponding to Ω_F are interacting at the common interface $\Gamma := \overline{\Omega}_F \cap \overline{\Omega}_S$. The elastic structure is fixed at $\Gamma_D \subseteq \partial\Omega_S$, that is, there is no displacement on this part of the boundary. A harmonic load acts on $\Gamma_N \subset \partial\Omega_S$. We have $\partial\Omega_S = \overline{\Gamma} \cup \overline{\Gamma}_D \cup \overline{\Gamma}_N$ and $\Gamma, \Gamma_D, \Gamma_N$ do not intersect each other and are relatively open. The boundary $\Gamma_W \subseteq \partial\Omega_F$ is assumed to be an acoustically hard wall, that is, the acoustic waves are totally reflected. With $\boldsymbol{n}_S$ we denote the outer normal vector on Ω_S and with $\boldsymbol{n}_F$ the outer normal vector on Γ_F and set $\boldsymbol{n} := \boldsymbol{n}_F = -\boldsymbol{n}_S$ (see Figure 1). We also define Ω open such that $\overline{\Omega} = \overline{\Omega}_F \cup \overline{\Omega}_S$, which is assumed to be Lipschitz and piecewise C^1 as well.

The displacements of the elastic structure $\boldsymbol{u} : \Omega_S \to \mathbb{C}^3$ and the pressure $p : \Omega_F \to \mathbb{C}$ in the fluid are then given for prescribed volume load $\boldsymbol{f} \in (L^2(\Omega_S))^3$ and surface load $\boldsymbol{g} \in (L^2(\Gamma_N))^3$ by the following system of partial differential equations.

$$-\Delta p - k^2 p = 0 \qquad \text{in } \Omega_F, \tag{2.1a}$$

$$-\operatorname{div} \sigma(\boldsymbol{u}) - \rho_S \omega^2 \boldsymbol{u} = \boldsymbol{f} \qquad \text{in } \Omega_S, \tag{2.1b}$$

$$\sigma(\boldsymbol{u})\boldsymbol{n} + p\boldsymbol{n} = 0 \qquad \text{on } \Gamma, \tag{2.1c}$$

$$\rho_F \omega^2 \boldsymbol{u} \cdot \boldsymbol{n} - \frac{\partial p}{\partial \boldsymbol{n}} = 0 \qquad \text{on } \Gamma, \tag{2.1d}$$

$$\frac{\partial p}{\partial \boldsymbol{n}} = 0 \qquad \text{on } \Gamma_W, \tag{2.1e}$$

$$\boldsymbol{u} = 0 \qquad \text{on } \Gamma_D, \tag{2.1f}$$

$$\sigma(\boldsymbol{u})\boldsymbol{n} = \boldsymbol{g} \qquad \text{on } \Gamma_N, \tag{2.1g}$$

where the stress tensor $\boldsymbol{\sigma}(\boldsymbol{u})$ is given by *Hooke's Law*

$$\sigma(\boldsymbol{u}) = \lambda \operatorname{trace} \varepsilon(\boldsymbol{u}) \boldsymbol{I} + 2\,\mu\varepsilon(\boldsymbol{u}), \tag{2.1h}$$

where $\lambda, \mu > 0$ are the material-dependent Lamé parameters, ρ_F, ρ_S are the densities of the fluid and structure, respectively, $k = \frac{\omega}{c}$, c is the speed of sound and $\omega > 0$ the angular frequency. The tensor $\varepsilon(\boldsymbol{u})$ in (2.1h) stands for the elastic strain and is given by

$$\varepsilon_{ij}(\boldsymbol{u}) = \frac{1}{2}(\partial_i \boldsymbol{u}_j + \partial_j \boldsymbol{u}_i) \quad i,j = 1,2,3.$$

equations (2.1c) and (2.1d) describe the coupling between the fluid and the solid on the common interface Γ. Equation (2.1c) is consequence of the fact that the pressure of the fluid on the solid is in equilibrium with the normal component of the stress in the solid, which is expressed by

$$\sigma(\boldsymbol{u})\boldsymbol{n}_S = p\,\boldsymbol{n}_F \Leftrightarrow \sigma(\boldsymbol{u})\boldsymbol{n} = -p\boldsymbol{n}.$$

on the common interface Γ, the displacement of the solid in normal direction is in equilibrium with the displacement in the fluid in normal direction. With the relation $\rho_F \omega^2 \boldsymbol{u}_F = \nabla p$, where

$\boldsymbol{u}_F$ is the displacement in the fluid and continuity of the displacement in normal direction $\boldsymbol{u}\cdot\boldsymbol{n} = \boldsymbol{u}_F\cdot\boldsymbol{n}$, we get the second interface condition

$$\rho_F\omega^2\boldsymbol{u}\cdot\boldsymbol{n} = \nabla p\cdot\boldsymbol{n} \quad \text{on}\,\Gamma.$$

For establishing the variational formulation of the problem, we introduce the space

$$\mathcal{H} := H^1(\Omega_F)\times\left(H^1_{\Gamma_D}(\Omega_S)\right)^3$$

equipped with the norm

$$\|(p,\boldsymbol{u})\|^2_{\mathcal{H}} := \|p\|^2_{H^1(\Omega_F)} + \|\boldsymbol{u}\|^2_{\left(H^1(\Omega_S)\right)^3}.$$

The variational formulation of (2.1) (for $\omega > 0$) is then: Find $(p,\boldsymbol{u})\in\mathcal{H}$, such that

$$B((p,\boldsymbol{u}),(q,\boldsymbol{v})) = L(q,\boldsymbol{v}) \quad \forall(q,\boldsymbol{v})\in\mathcal{H}, \tag{2.2}$$

where

$$\begin{aligned} B((p,\boldsymbol{u}),(q,\boldsymbol{v})) = {} & B_F(p,q) - \rho_F\omega^2 B_{FS}((p,\boldsymbol{u}),(q,\boldsymbol{v})) \\ & - \rho_F\omega^2 B^*_{FS}((p,\boldsymbol{u}),(q,\boldsymbol{v})) + \rho_F\omega^2 B_S(\boldsymbol{u},\boldsymbol{v}) \end{aligned} \tag{2.3}$$

with

$$\begin{aligned} B_F(p,q) &= \int_{\Omega_F}\nabla p\cdot\nabla\overline{q}\,\mathrm{d}x - \frac{\omega^2}{c^2}\int_{\Omega_F} p\overline{q}\,\mathrm{d}x, \\ B_{FS}((p,\boldsymbol{u}),(q,\boldsymbol{v})) &= \int_\Gamma(\boldsymbol{u}\cdot\boldsymbol{n})\overline{q}\,\mathrm{d}\sigma, \\ B^*_{FS}((p,\boldsymbol{u}),(q,\boldsymbol{v})) &= \overline{B_{FS}((q,\boldsymbol{v}),(p,\boldsymbol{u}))} = \int_\Gamma p\left(\boldsymbol{n}\cdot\overline{\boldsymbol{v}}\right)\mathrm{d}\sigma, \\ B_S(\boldsymbol{u},\boldsymbol{v}) &:= \int_{\Omega_S}\sigma(\boldsymbol{u}) : \varepsilon\left(\overline{\boldsymbol{v}}\right)\mathrm{d}x - \omega^2\int_{\Omega_S}\rho_S\boldsymbol{u}\cdot\overline{\boldsymbol{v}}\,\mathrm{d}x, \end{aligned}$$

where the bar denotes the complex conjugate, and

$$L((q,\boldsymbol{v})) = \rho_F\omega^2\left(\int_{\Omega_S}\boldsymbol{f}\cdot\overline{\boldsymbol{v}}\,\mathrm{d}x + \int_{\Gamma_N}\boldsymbol{g}\cdot\overline{\boldsymbol{v}}\,\mathrm{d}\sigma\right).$$

Remark 2.1. *The coupling conditions (2.1c), (2.1d) take the same form regardless of whether the normal vector points into the structure, as we assumed, or into the fluid. This is not anymore the case for the variational formulation (2.3), and the sign in front of B_{FS} and B^*_{FS} becomes a minus if the normal vector points into the fluid. This means that the normal vector in Barucq et al. (2014), where it was not indicated, points into the fluid. In Stammberger and Voss (2014), the same direction was assumed but due to the wrong sign a physically not correct solution was considered.*

3. Existence and uniqueness

The Lax–Milgram lemma cannot be applied as this problem is not elliptic. Nevertheless, it has a unique solution up to some values of the frequency $\omega > 0$ as stated in the following theorem and proved based on the Fredholm–Riesz–Schauder theory.

Theorem 3.1. *Let $\boldsymbol{f}\in(L^2(\Omega_S))^3$ and $\boldsymbol{g}\in(L^2(\Gamma))^3$, then up to countably many values of $\omega > 0$, whose only possible accumulation point is infinity, the problem (2.2) has a unique solution $(p,\boldsymbol{u})\in\mathcal{H}$ with*

$$\|(p,\boldsymbol{u})\|_{\mathcal{H}} \le C\left(\|\boldsymbol{f}\|_{\left(L^2(\Omega_S)\right)^3} + \|\boldsymbol{g}\|_{\left(L^2(\Gamma_N)\right)^3}\right). \tag{3.1}$$

Proof. The proof is based on the Fredholm–Riesz–Schauder theory (Sauter and Schwab, 2011, Sec. 2.1.4). The symmetric variational formulation (2.2) is quadratic in ω^2. To obtain an equivalent formulation that is linear in ω^2, we insert as test functions $(q/\rho_F, \boldsymbol{v}/(\rho_F\omega^2))$ leading to

$$\frac{1}{\rho_F}\int_{\Omega_F} \nabla p\cdot\nabla\overline{q} - \frac{\omega^2}{c^2} p\overline{q}\,\mathrm{d}x - \omega^2\int_\Gamma \boldsymbol{u}\cdot\boldsymbol{n}\,\mathrm{d}\sigma - \int_\Gamma p\overline{\boldsymbol{v}}\cdot\boldsymbol{n}\,\mathrm{d}\sigma + \int_{\Omega_S}\sigma(\boldsymbol{u}):\varepsilon(\overline{\boldsymbol{v}}) - \omega^2\rho_S\boldsymbol{u}\cdot\overline{\boldsymbol{v}}\,\mathrm{d}x$$
$$= \int_{\Omega_S}\boldsymbol{f}\cdot\overline{\boldsymbol{v}}\,\mathrm{d}x + \int_{\Gamma_N}\boldsymbol{g}\cdot\boldsymbol{v}\,\mathrm{d}\sigma.$$

Now, we define the Hilbert space operators $A, M : \mathcal{H}\to\mathcal{H}$ by

$$(A(p,\boldsymbol{u}),(q,\boldsymbol{v}))_{\mathcal{H}} = \frac{1}{\rho_F}\int_{\Omega_F}\nabla p\cdot\nabla\overline{q} + \frac{1}{c^2}p\overline{q}\,\mathrm{d}x + \int_{\Omega_S}\sigma(\boldsymbol{u}):\varepsilon(\overline{\boldsymbol{v}}) + \rho_S\boldsymbol{u}\cdot\overline{\boldsymbol{v}}\,\mathrm{d}x + \int_\Gamma(\boldsymbol{u}\cdot\boldsymbol{n})\overline{q} - p(\overline{\boldsymbol{v}}\cdot\boldsymbol{n})\,\mathrm{d}\sigma$$
$$(M(p,\boldsymbol{u}),(q,\boldsymbol{v}))_{\mathcal{H}} = \frac{1}{\rho_F c^2}\int_{\Omega_F} p\overline{q}\,\mathrm{d}x + \int_{\Omega_S}\rho_S\boldsymbol{u}\cdot\overline{\boldsymbol{v}}\,\mathrm{d}x + \int_\Gamma(\boldsymbol{u}\cdot\boldsymbol{n})\overline{q}\,\mathrm{d}\sigma$$

for all $(q,\boldsymbol{v})\in\mathcal{H}$, which exist by Riesz representation theorem when the Hilbert space $\mathcal{H}$ is equipped with the inner product

$$((p,\boldsymbol{u}),(q,\boldsymbol{v}))_{\mathcal{H}} = (p,q)_{H^1(\Omega_F)} + (\boldsymbol{u},\boldsymbol{v})_{\left(H^1(\Omega_S)\right)^3}.$$

Then the variational formulation (2.2) is equivalent (for $\omega > 0$) to the operator equation

$$\left(A - \left(\omega^2+1\right)M\right)(p,\boldsymbol{u}) = F. \tag{3.2}$$

here, we define $F\in\mathcal{H}$ by the Riesz isomorphism

$$(F,(q,\boldsymbol{v}))_{\mathcal{H}} = \int_{\Omega_S}\boldsymbol{f}\cdot\overline{\boldsymbol{v}}\,\mathrm{d}x + \int_{\Gamma_N}\boldsymbol{g}\cdot\overline{\boldsymbol{v}}\,\mathrm{d}\sigma \quad \forall(q,\boldsymbol{v})\in\mathcal{H},$$

which is a proper definition since the two integrals are bounded for all $\boldsymbol{v}\in(H^1(\Omega_S))^3$.
By Korn's inequality (see Ciarlet, 1988, Theorem 6.3–3), the operator A is an isomorphism as it is continuous and has a continuous inverse by the Lax–Milgram lemma using the $\mathcal{H}$-ellipticity

$$\mathrm{Re}(A(p,\boldsymbol{u}),(p,\boldsymbol{u}))_{\mathcal{H}} = \frac{1}{\rho_F}|p|^2_{H^1(\Omega_F)} + \frac{1}{\rho_F c^2}\|p\|^2_{L^2(\Omega_F)} + \int_{\Omega_S}\sigma(\boldsymbol{u}):\varepsilon(\overline{\boldsymbol{u}})\mathrm{d}x + \|\sqrt{\rho_S}\boldsymbol{u}\|^2_{\left(L^2(\Omega_S)\right)^3} \ge \gamma\|(p,\boldsymbol{u})\|^2_{\mathcal{H}}$$

for all $(p,\boldsymbol{u})\in\mathcal{H}$ and some $\gamma > 0$.
We show now that the operator M is compact. For any bounded sequence $(p_n,\boldsymbol{u}_n)_{n\in\mathbb{N}}\in\mathcal{H}$, there exists a subsequence, again denoted by $(p_n,\boldsymbol{u}_n)_{n\in\mathbb{N}}$, that is weakly converging to $(p,\boldsymbol{u})$ in $\mathcal{H}$. For the sequence $(M(p_n,\boldsymbol{u}_n))_{n\in\mathbb{N}}$ in $\mathcal{H}$, we find that

$$\|M(p-p_n,\boldsymbol{u}-\boldsymbol{u}_n)\|_{\mathcal{H}}^2=(M(p-p_n,\boldsymbol{u}-\boldsymbol{u}_n),M(p-p_n,\boldsymbol{u}-\boldsymbol{u}_n))_{\mathcal{H}}$$

$$=\left(\frac{1}{\rho_F c^2}\int_{\Omega_F}(p-p_n)\overline{q}\,\mathrm{d}x+\int_{\Omega_S}\rho_S(\boldsymbol{u}-\boldsymbol{u}_n)\cdot\overline{\boldsymbol{v}}\,\mathrm{d}x+\int_{\Gamma}((\boldsymbol{u}-\boldsymbol{u}_n)\cdot\boldsymbol{n})\overline{q}\,\mathrm{d}\sigma\right)\Bigg|_{(q,\boldsymbol{v})=M(p-p_n,\boldsymbol{u}-\boldsymbol{u}_n)}.$$

and with the Cauchy–Schwarz inequality, cancelling $\|M(p-p_n,\boldsymbol{u}-\boldsymbol{u}_n)\|_{\mathcal{H}}$ on both sides and by the trace theorem for functions in $H^{1/2}(\Omega_S)$ for some constant C, see McLean(2000, Theorem 3.38).

$$\begin{aligned}\|M(p-p_n,\boldsymbol{u}-\boldsymbol{u}_n)\|_{\mathcal{H}} &\leq \frac{1}{\rho_F c^2}\|p-p_n\|_{L^2(\Omega_F)}+\|\rho_S(\boldsymbol{u}-\boldsymbol{u}_n)\|_{\left(L^2(\Omega_S)\right)^3}+\rho_F\|\boldsymbol{u}\cdot\boldsymbol{n}-\boldsymbol{u}_n\cdot\boldsymbol{n}\|_{H^{-1/2}(\Gamma)}\\ &\leq C\left(\|p-p_n\|_{L^2(\Omega_F)}+\|\boldsymbol{u}-\boldsymbol{u}_n\|_{\left(H^{1/2}(\Omega_S)\right)^3}\right).\end{aligned}\tag{3.3}$$

Due to the compact embeddings $H^1(\Omega_F)\subset\subset L^2(\Omega_F)$ and $H^1(\Omega_S)\subset\subset H^{1/2}(\Omega_S)$ by the Rellich–Kondrachov compactness theorem (Evans, 2010), the right-hand side of (3.3) converges to 0; hence, the sequence $(M(p_n,\boldsymbol{u}_n))_{n\in\mathbb{N}}$ in $\mathcal{H}$ converges to $M(p,\boldsymbol{u})\in\mathcal{H}$ and M is compact.

Denoting $\lambda=1/(\omega^2+1)<1$, $T:=A^{-1}M$ and the identity operator I in $\mathcal{H}$, the operator equation (3.2) is equivalent to

$$(\lambda I-T)(p,\boldsymbol{u})=\lambda A^{-1}F.$$

Since T is compact due to the compactness of M (Sauter and Schwab, 2011), the equation is well-posed by the Fredholm–Riesz–Schauder theory except for countably many eigenvalues λ whose only possible accumulation point is zero (Sauter and Schwab, 2011, Theorem 2.1.36). Hence (3.2) and in turn (2.2) are well-defined except for countably many values ω whose only possible accumulation point is infinity.

This completes the proof of the theorem.

Remark 3.2. *The statement of Theorem 3.1 and the proof can be easily extended to the case of radiation conditions in an unbounded (fluid) domain, for which it simplifies much the proof given in Barucq et al. (2014), or to the cases of absorption in the domain or through Robin boundary conditions. With them the formulation is only perturbed in the main part corresponding to the operator A and additional terms of lower order appear in the formulation that can be integrated in the operator M. In Stammberger and Voss (2014), the spectral properties of the associated eigenvalue problem for the case without absorption were shown – it has only nonnegative positive eigenvalues ω^2 – where the idea of the proof does not seem to be directly extendable to the source problem with absorption.*

4. Shape optimization

In this section, we first describe the main tools used to study the sensibility of a cost functional depending on the shape of the elastic structure. We compute the so-called *distributed shape derivative* (Berggren, 2010; Hiptmair *et al.*, 2015; Laurain and Sturm, 2016;

Laurain, 2020) (see also Delfour and Zolésio (2011), Sokolowski and Zolesio (1992), Henrot and Pierre (2018) for boundary expressions of shape derivatives) in an infinite-dimensional setting, for some reference domain Ω and free-form regular perturbations. This allows to obtain a descent direction for an optimization algorithm in the infinite-dimensional setting. In the numerical part we specialize to particular perturbations, and we use a discretized descent direction. We first introduce the *geometric flow* of a domain Ω, then we recall some fundamental calculus lemmas and the averaged adjoint method introduced in Sturm (2015), see also Laurain and Sturm (2016), that we use to compute the distributed shape derivative.

4.1 Preliminaries

We start with a general description of the shape optimization theory. Let $\mathfrak{D} \subseteq \mathbb{R}^3$ be a bounded open set and $\mathcal{P}(\mathfrak{D})$ be the set of all subsets of $\mathfrak{D}$. In shape optimization, one considers *shape functionals* $J : \mathcal{U}_{ad} \to \mathbb{R}$, where $\mathcal{U}_{ad} \subset \mathcal{P}(\mathfrak{D})$ is a set of admissible shapes, that is, subsets of $\mathfrak{D}$ satisfying certain constraints, such as regularity or geometric constraints. For the particular problem under consideration in this paper, $\mathfrak{D}$ contains all admissible sets $\Omega_F \cup \Omega_S$ required for the optimization; see Section 4.3 for more details. Let us assume that the infimum of J is attained over $\mathcal{U}_{ad}$. Our aim is to effectively determine a set Ω^* such that

$$J(\Omega^*) = \min_{\Omega \in \mathcal{U}_{ad}} J(\Omega).$$

Usually, an approximation of Ω^* can be found by means of a numerical method.

To devise an algorithm for minimizing J, one needs to compute derivatives of J. However, even though topologies can be defined for the shape space $\mathcal{U}_{ad}$, it is usually not a vector space, and it is not clear how to define differentiation. In order to obtain a notion of derivative for shape functionals, we consider perturbations of a reference domain Ω using the flow $\Phi_t^{\boldsymbol{\theta}} : \overline{\mathfrak{D}} \to \mathbb{R}^3$ for $t \in [0, \tau]$, for some $\tau > 0$, of a given vector field $\boldsymbol{\theta} \in \mathcal{D}^k(\mathfrak{D}, \mathbb{R}^3)$, $k \geq 1$ or $k = \infty$, where $\mathcal{D}^k(\mathfrak{D}, \mathbb{R}^3)$ is defined as:

$$\mathcal{D}^k(\mathfrak{D}, \mathbb{R}^3) := \{w \in C^k(\mathfrak{D}, \mathbb{R}^3) | \quad \overline{\{x \in \mathbb{R}^3 : \ w \neq 0\}} \subset \mathfrak{D}\}.$$

For each $\boldsymbol{x}_0 \in \overline{\mathfrak{D}}$, the flow $\Phi_t^{\boldsymbol{\theta}}(\boldsymbol{x}_0) := \boldsymbol{x}(t)$ solves.

$$\dot{\boldsymbol{x}}(t) = \boldsymbol{\theta}(\boldsymbol{x}(t)) \quad \text{in } [0, \tau], \tag{4.1a}$$

$$\boldsymbol{x}(0) = \boldsymbol{x}_0. \tag{4.1b}$$

Note that $D\Phi_0^{\boldsymbol{\theta}} = \mathrm{Id}$ and $\det D\Phi_0^{\boldsymbol{\theta}} = 1$ are independent of $\boldsymbol{\theta}$. In the following we write $\boldsymbol{\Phi}_t$ instead of $\Phi_t^{\boldsymbol{\theta}}$ for the sake of simplicity. Using this flow we consider a variation $\Omega^t := \boldsymbol{\Phi}_t(\Omega)$ of the initial shape Ω.

Definition 4.1. Let $J : \mathcal{P}(\mathfrak{D}) \to \mathbb{R}$ be a shape functional and $k \geq 1$. The Eulerian semiderivative in direction $\boldsymbol{\theta} \in \mathcal{D}^k(\mathfrak{D}, \mathbb{R}^3)$ is defined by, when the limit exists,

$$dJ(\Omega; \boldsymbol{\theta}) := \lim_{t \searrow 0} \frac{J(\Omega^t) - J(\Omega)}{t}.$$

The functional J is said to be shape differentiable at Ω if it has a Eulerian semiderivative at Ω for all $\boldsymbol{\theta} \in \mathcal{D}^\infty(\mathfrak{D}, \mathbb{R}^3)$ and the mapping

$$dJ(\Omega) : \mathcal{D}^{\infty}\left(\mathfrak{D}, \mathbb{R}^3\right) \to \mathbb{R}, \ \boldsymbol{\theta} \mapsto dJ(\Omega; \boldsymbol{\theta})$$

is linear and continuous, in which case $dJ(\Omega; \boldsymbol{\theta})$ *is called the shape derivative of* J *at* Ω *in direction* $\boldsymbol{\theta}$.

For the actual minimization of J, we need to compute appropriate descent directions.

Definition 4.2. *A vector field* $\boldsymbol{\theta} \in \mathcal{D}^k(\mathfrak{D}, \mathbb{R}^3)$, $k \geq 1$, *is called descent direction of* J *at* Ω, *if there exists a* $\bar{t}$, *such that*

$$J\left(\Omega^t\right) < J(\Omega) \quad \text{for all } t \in \left(0, \bar{t}\right],$$

where $\Omega^t := \Phi_t^{\boldsymbol{\theta}}(\Omega)$.

According to Definition 4.2, if J is shape differentiable at Ω, then $\boldsymbol{\theta}$ is a descent direction if $dJ(\Omega; \boldsymbol{\theta}) < 0$.

We recall two standard results for shape derivatives, which will be useful later on.

Lemma 4.3. *Let* $\Omega \subset \mathfrak{D}$ *be a Lipschitz domain,* $f \in W^{1,1}(\mathfrak{D})$ *and* $g \in H^2(\mathbb{R}^3)$. *We have*

$$\int_{\Phi_t(\Omega)} f \, \mathrm{d}x = \int_{\Omega} f \circ \Phi_t \, j(t) \, \mathrm{d}x, \tag{4.2}$$

$$\int_{\Phi_t(\partial\Omega)} g \, \mathrm{d}\sigma = \int_{\partial\Omega} g \circ \Phi_t \, j_{\Gamma}(t) \, \mathrm{d}\sigma, \tag{4.3}$$

with the Jacobian $j(t) = |\det D\boldsymbol{\Phi}_t|$ *and the tangential Jacobian*

$$j_{\Gamma}(t) = \left|\det(D\Phi_t)(D\Phi_t)^{-T}\boldsymbol{n}\right| = j(t)\left|(D\Phi_t)^{-T}\boldsymbol{n}\right|.$$

We also have

$$(\nabla f) \circ \Phi_t = (D\Phi_t)^{-T} \nabla (f \circ \Phi_t). \tag{4.4}$$

Proof. See Henrot and Pierre (2018, Theorem 5.2.2) and Delfour and Zolésio (2011, Chapter 9, section 4.2).

For C^2-domains, the outward normal vector to Ω^t can be related to the normal vector to Ω via a simple formula; see Delfour and Zolésio (2011, Theorem 4.4, Chap. 9). This result can be extended to Lipschitz domains with piecewise C^1 boundary as follows.

Lemma 4.4. *Let* $\Omega \subset \mathbb{R}^3$ *be a Lipschitz domain with piecewise* C^1 *boundary and* $\Phi_t = \Phi_t^{\boldsymbol{\theta}}$ *with* $\boldsymbol{\theta}$ *in* $\mathcal{D}^k(\mathfrak{D}, \mathbb{R}^3)$, $k \geq 1$. *Denote* $S_{\Omega} \subset \partial\Omega$ *the finite set of points where* Ω *is not* C^1. *Let* $\boldsymbol{n}$ *be the outer normal vector to* Ω *on* $\partial\Omega \backslash S_{\Omega}$ *and* $\boldsymbol{n}_t$ *be the outer normal vector to* $\boldsymbol{\Phi}_t(\Omega)$ *on* $\boldsymbol{\Phi}_t(\partial\Omega \backslash S_{\Omega})$. *Then we have*

$$\boldsymbol{n}_t \circ \Phi_t = \frac{(D\Phi_t)^{-T}\boldsymbol{n}}{\left|(D\Phi_t)^{-T}\boldsymbol{n}\right|} \text{ on } \partial\Omega \backslash S_{\Omega}. \tag{4.5}$$

We will also need the following basic results and notations for tensor calculus.

Notations. For sufficiently smooth $\Omega \subset \mathbb{R}^d$, vector-valued functions $\boldsymbol{a}, \boldsymbol{b} : \mathbb{R}^d \to \mathbb{R}^d$ and a second-order tensor $\mathbf{S} : \mathbb{R}^d \to \mathbb{R}^{d \times d}$, we use the following notations.

(1) $\boldsymbol{I}$ *for the identity matrix in* $\mathbb{R}^{d\times d}$.

(2) Id: $x \mapsto x$ *for the identity in* $\mathbb{R}^d$.

(3) $\boldsymbol{a}\otimes\boldsymbol{b}$ *for the outer product of* $\boldsymbol{a}$ *and* $\boldsymbol{b}$.

(4) $\boldsymbol{a}\odot\boldsymbol{b} := \frac{1}{2}(\boldsymbol{a}\otimes\boldsymbol{b} + \boldsymbol{b}\otimes\boldsymbol{a})$ *for the symmetric outer product of* $\boldsymbol{a}$ *and* $\boldsymbol{b}$.

(5) $D_\Gamma \boldsymbol{a} := D\boldsymbol{a} - (D\boldsymbol{a})\boldsymbol{n}\otimes\boldsymbol{n}$ *for the tangential derivative on* $\partial\Omega$.

(6) $\mathrm{div}_\Gamma \boldsymbol{a} := \mathrm{div}\,\boldsymbol{a} - (D\boldsymbol{a})\boldsymbol{n}\cdot\boldsymbol{n}$ *for the tangential divergence on* $\partial\Omega$.

(7) $\mathrm{div}(\mathbf{S})$ *is defined as the vector of the divergence of the rows of* $\mathbf{S}$.

Lemma 4.5. (Tensor calculus). For sufficiently smooth vector-valued functions $\boldsymbol{a}, \boldsymbol{b} : \mathbb{R}^d \to \mathbb{R}^d$ *and a second-order tensor* $\mathbf{S} : \mathbb{R}^d \to \mathbb{R}^{d\times d}$, *we have* $\mathbf{S} : (\boldsymbol{a}\otimes\boldsymbol{b}) = \boldsymbol{a}\cdot\mathbf{S}\boldsymbol{b} = \mathbf{S}^\mathsf{T}\boldsymbol{a}\cdot\boldsymbol{b} = \mathbf{S}^\mathsf{T} : (\boldsymbol{b}\otimes\boldsymbol{a})$.

4.2 Averaged adjoint method

There exist several methods to prove the shape differentiability of cost functionals depending on the solution of a PDE. Established methods comprise the material/shape derivative method (Sokolowski and Zolesio, 1992), methods based on the implicit function theorem (Laurain *et al.*, 2020), the min approach for energy cost functions (Delfour, 2012), a penalization method (Delfour and Zolésio, 1988a) and rearrangement methods (Ito *et al.*, 2008; Kasumba and Kunisch, 2011, 2014). Lagrangian methods are convenient as they allow for a direct calculation of the adjoint. The formal Lagrangian method of Céa is frequently used; see Céa (1986), Pantz (2005). In this paper, we use the averaged adjoint method (Sturm, 2015; Laurain and Sturm, 2016), which generalizes the minimax approach of Delfour and Zolésio (1988b) and simplifies its assumptions.

We now briefly describe the averaged adjoint method as introduced in Sturm (2015). Let two vector spaces $E = E(\Omega)$, $F = F(\Omega)$ and $\tau > 0$ be given, and consider a parameterization $\Omega^t = \Phi_t(\Omega)$ for $t \in [0,\tau]$. Our goal is to differentiate shape functions of the type $J(\Omega^t)$ that can be written using a Lagrangian as $J(\Omega^t) = \mathcal{L}(\Omega^t, u^t, \widehat{\psi})$, where $u^t \in E(\Omega^t)$ and $\widehat{\psi} \in F(\Omega^t)$. Since $\mathcal{L}(\Omega^t, \widehat{\varphi}, \widehat{\psi})$ usually consists of integrals on $\Phi_t(\Omega)$, a change of variables allows to pull these integrals back to the reference domain Ω and consequently to transfer the dependence on t to the integrand. However, in the process appear the functions $\widehat{\varphi}\circ\Phi_t \in E(\Omega)$ and $\widehat{\psi}\circ\Phi_t \in F(\Omega)$, which are impractical to differentiate since $\widehat{\varphi}$ and $\widehat{\psi}$ are defined on the moving spaces $E(\Omega^t)$ and $F(\Omega^t)$. To circumvent this problem, one works with the reparameterization $\mathcal{L}(\Omega^t, \varphi\circ\Phi_t^{-1}, \psi\circ\Phi_t^{-1})$ instead of $\mathcal{L}(\Omega^t, \widehat{\varphi}, \widehat{\psi})$, with $\varphi \in E(\Omega)$ and $\psi \in F(\Omega)$. In this way, after the change of variables in the integrals, the integrand depends on φ and ψ, which are defined on spaces independent of t. In the present paper, both E and F correspond to $\mathcal{H}$.

Thus, we consider Lagrangian-type functions $G : [0,\tau]\times E\times F \to \mathbb{R}$ with

$$G(t,\varphi,\psi) := \mathcal{L}\big(\Phi_t(\Omega), \varphi\circ\Phi_t^{-1}, \psi\circ\Phi_t^{-1}\big).$$

Theorem 4.8 shows that the shape derivative of $\mathcal{L}$ corresponds to the partial derivative with respect to t of G with φ equal to the state and ψ to the adjoint. The main ingredient is the so-called averaged adjoint equation that we introduce further. In this paper, we take $E = \Pi_{i=1}^m E_i$ and $F = \Pi_{i=1}^m F_i$, $m \in \mathbb{N}^*$, to be Cartesian products of vector spaces. We also consider the particular case

$$G(t,\varphi,\psi) := a(t,\varphi,\psi) + b(t,\varphi), \tag{4.6}$$

where $a : [0, \tau] \times E \times F \to \mathbb{R}$ and $b : [0, \tau] \times E \to \mathbb{R}$ are functions such that $\psi \mapsto a(t, \varphi, \psi)$ is linear for all $t \in [0, \tau]$ and $\varphi \in E$. The function G is called *shape-Lagrangian*, while b and a correspond to the objective function and to the constraint, respectively. Throughout the paper, the Greek letters φ and ψ are used for variables, while the Gothic letters $\mathfrak{e}$, $\mathfrak{f}$ are used for the solutions of the state and adjoint states, respectively.

Let us assume that for each $t \in [0, \tau]$ the equation

$$d_\psi G\left(t, \mathfrak{e}^t, 0; \widehat{\psi}\right) = a\left(t, \mathfrak{e}^t, \widehat{\psi}\right) = 0 \quad \text{for all } \widehat{\psi} \in F. \tag{4.7}$$

admits a unique solution $\mathfrak{e}^t \in E$. We make the following assumptions about G.

Assumption 4.6. For every $(t, \psi) \in [0, \tau] \times F$, we have that

(1) $[0, 1] \ni s \mapsto G(t, s\mathfrak{e}^t + (1-s)\mathfrak{e}^0, \psi)$ *is absolutely continuous;*

(2) $[0, 1] \ni s \mapsto d_\varphi G(t, s\mathfrak{e}^t + (1-s)\mathfrak{e}^0, \psi; \widehat{\varphi})$ *belongs to* $L^1(0, 1)$ *for all* $\widehat{\varphi} \in E$.

When Assumption 4.6 is satisfied, for $t \in [0, \tau]$ we introduce the *averaged adjoint equation* associated with $\mathfrak{e}^t$ and $\mathfrak{e}^0$: find $\mathfrak{f}^t \in F$ such that

$$\int_0^1 d_\varphi G\left(t, s\mathfrak{e}^t + (1-s)\mathfrak{e}^0, \mathfrak{f}^t; \widehat{\varphi}\right) ds = 0 \quad \text{for all } \widehat{\varphi} \in E. \tag{4.8}$$

Assumption 4.6(2) implies that for all $t \in [0, \tau]$ we have

$$G\left(t, \mathfrak{e}^t, \mathfrak{f}^t\right) - G\left(t, \mathfrak{e}^0, \mathfrak{f}^t\right) = \int_0^1 d_\varphi G\left(t, s\mathfrak{e}^t + (1-s)\mathfrak{e}^0, \mathfrak{f}^t; \mathfrak{e}^t - \mathfrak{e}^0\right) ds = 0. \tag{4.9}$$

Assumption 4.7. We assume that

$$\lim_{t \searrow 0} \frac{G\left(t, \mathfrak{e}^0, \mathfrak{f}^t\right) - G\left(0, \mathfrak{e}^0, \mathfrak{f}^t\right)}{t} = \partial_t G\left(0, \mathfrak{e}^0, \mathfrak{f}^0\right).$$

We can now state the main result of the averaged adjoint method.

Theorem 4.8. Suppose that Assumptions 4.6 and 4.7 hold, and that there exists a unique solution $\mathfrak{f}^t$ of the averaged adjoint equation (4.8) for all $t \in [0, \tau]$. Then for any $\psi \in F$ we obtain

$$\frac{d}{dt} b\left(t, \mathfrak{e}^t\right)|_{t=0} = \frac{d}{dt} \left(G\left(t, \mathfrak{e}^t, \psi\right)\right)|_{t=0} = \partial_t G\left(0, \mathfrak{e}^0, \mathfrak{f}^0\right). \tag{4.10}$$

4.3 Shape optimization problem

For the problem under consideration in this paper, $\mathfrak{D} \subset \mathbb{R}^3$ is an open set containing all admissible sets Ω_F and Ω_S; see Section 2 for a description of the geometry. In fact, we have two variable domains (Ω_F, Ω_S), so we are in a slightly more general situation than the material presented in Section 4.1, but the generalization is straightforward. Thus, here $\mathcal{U}_{ad} \subset \mathcal{P}(\mathfrak{D}) \times \mathcal{P}(\mathfrak{D})$ is a subset of admissible pairs of Lipschitz, piecewise C^1 domains (Ω_F, Ω_S), which satisfy the geometric constraints described in Section 2. In Section 4.6, we derive a general formula for the shape derivative, valid for a large range of domain transformations. In our numerical application, we consider translations of subsets of Ω_F and Ω_S. This corresponds to the positioning of a bead on a thin plate in order to reduce the noise of the fluid area.

Our aim is to minimize the shape functional $J : \mathcal{U}_{ad} \to \mathbb{R}$ given by

$$J(\Omega_F, \Omega_S) := \int_{\Omega_F} \kappa |p(\Omega_F, \Omega_S) - p_d|^2 \, \mathrm{d}x, \tag{4.11}$$

with the constraint that the pressure $p = p(\Omega_F, \Omega_S)$ is the solution of (2.1) for a fixed frequency ω. Here, $\kappa \in C^\infty(\mathfrak{D})$ is a weighting function defining the location of the optimization and $p_d : \mathfrak{D} \to \mathbb{R}$ is a prescribed pressure distribution.

Let us introduce a Lagrangian $\mathcal{L} : \mathcal{U}_{ad} \times \mathcal{H} \times \mathcal{H} \to \mathbb{R}$ that combines the cost functional and the weak formulation of the PDE constraint. Although the PDE constraint (2.2) is complex-valued, it is sufficient to include only the real part of the PDE in the Lagrangian. Indeed, the complex-valued PDE (2.2) can be recovered by choosing appropriate test functions; see Hintermüller *et al.* (2015) for details. Thus we define

$$\begin{aligned}\mathcal{L}((\Omega_F, \Omega_S), (\mathfrak{p}, \mathfrak{u}), (\mathfrak{q}, \mathfrak{v})) = \int_{\Omega_F} \kappa |\mathfrak{p} - p_d|^2 \, \mathrm{d}x + \mathrm{Re}\Bigg(\int_{\Omega_F} \nabla \mathfrak{p} \cdot \nabla \overline{\mathfrak{q}} \, \mathrm{d}x - \frac{\omega^2}{c^2} \int_{\Omega_F} \mathfrak{p} \overline{\mathfrak{q}} \, \mathrm{d}x \\ - \rho_F \omega^2 \int_\Gamma (\mathfrak{u} \cdot \boldsymbol{n}) \overline{\mathfrak{q}} \, \mathrm{d}\sigma - \rho_F \omega^2 \int_\Gamma \mathfrak{p} \left(\boldsymbol{n} \cdot \overline{\mathfrak{v}} \right) \mathrm{d}\sigma \\ + \rho_F \omega^2 \int_{\Omega_S} \sigma(\mathfrak{u}) : \varepsilon\left(\overline{\mathfrak{v}} \right) \mathrm{d}x - \rho_F \rho_S \omega^4 \int_{\Omega_S} \mathfrak{u} \cdot \overline{\mathfrak{v}} \, \mathrm{d}x \\ - \rho_F \omega^2 \int_{\Omega_S} \boldsymbol{f} \cdot \overline{\mathfrak{v}} \, \mathrm{d}x - \rho_F \omega^2 \int_{\Gamma_N} \boldsymbol{g} \cdot \overline{\mathfrak{v}} \, \mathrm{d}\sigma \Bigg),\end{aligned}$$

where $(\mathfrak{p}, \mathfrak{u}), (\mathfrak{q}, \mathfrak{v}) \in \mathcal{H}$. The key feature of the Lagrangian method is that J satisfies

$$J(\Omega_F, \Omega_S) = \mathcal{L}((\Omega_F, \Omega_S), (p, \boldsymbol{u}), (\mathfrak{q}, \mathfrak{v})), \qquad \forall (\mathfrak{q}, \mathfrak{v}) \in \mathcal{H}.$$

The state $(p, \boldsymbol{u})$ and adjoint state $(q, \boldsymbol{v})$ are solutions of, respectively.

$$D_{(\mathfrak{q},\mathfrak{v})} \mathcal{L}(\Omega_F, \Omega_S, (p, \boldsymbol{u}), (0, \boldsymbol{0})) \left(\widehat{q}, \widehat{\boldsymbol{v}} \right) = 0 \text{ for all } \left(\widehat{q}, \widehat{\boldsymbol{v}} \right) \in \mathcal{H}, \tag{4.12}$$

$$D_{(\mathfrak{p},\mathfrak{u})} \mathcal{L}(\Omega_F, \Omega_S, (p, \boldsymbol{u}), (q, \boldsymbol{v})) \left(\widehat{p}, \widehat{\boldsymbol{u}} \right) = 0 \text{ for all } \left(\widehat{p}, \widehat{\boldsymbol{u}} \right) \in \mathcal{H}. \tag{4.13}$$

Choosing first purely real and then purely imaginary test functions (4.12) yields the weak form (2.2) of the state equation. Proceeding in the same way for (4.13) leads to the following weak formulation of the adjoint system

$$\begin{aligned}D_{(\mathfrak{p},\mathfrak{u})} \mathcal{L}(\Omega_F, \Omega_S, (p, \boldsymbol{u}), (q, \boldsymbol{v})) \left(\widehat{p}, \widehat{\boldsymbol{u}} \right) = \int_{\Omega_F} 2\kappa \left(\overline{p} - \overline{p}_d \right) \widehat{p} \, \mathrm{d}x + \int_{\Omega_F} \nabla \widehat{p} \cdot \nabla \overline{q} \, \mathrm{d}x - \frac{\omega^2}{c^2} \int_{\Omega_F} \widehat{p} \overline{q} \, \mathrm{d}x \\ - \rho_F \omega^2 \int_\Gamma \left(\overline{\boldsymbol{v}} \cdot \boldsymbol{n} \right) \widehat{p} \, \mathrm{d}\sigma - \rho_F \omega^2 \int_\Gamma \overline{q} \left(\boldsymbol{n} \cdot \widehat{\boldsymbol{u}} \right) \mathrm{d}\sigma \\ + \rho_F \omega^2 \int_{\Omega_S} \sigma\left(\widehat{\boldsymbol{u}} \right) : \varepsilon\left(\overline{\boldsymbol{v}} \right) \mathrm{d}x - \rho_F \rho_S \omega^4 \int_{\Omega_S} \widehat{\boldsymbol{u}} \cdot \overline{\boldsymbol{v}} \, \mathrm{d}x = 0.\end{aligned} \tag{4.14}$$

The corresponding strong form of the adjoint system is given by

$$\begin{aligned}
-\Delta q - \frac{\omega^2}{c^2} q &= -2\kappa(p - p_d) && \text{in } \Omega_F,\\
-\operatorname{div} \sigma(\boldsymbol{v}) - \rho_S \omega^2 \boldsymbol{v} &= 0 && \text{in } \Omega_S\\
\sigma(\boldsymbol{v})\boldsymbol{n} + q\boldsymbol{n} &= 0 && \text{on } \Gamma,\\
\rho_F \omega^2 \boldsymbol{v}\cdot\boldsymbol{n} - \frac{\partial q}{\partial \boldsymbol{n}} &= 0 && \text{on } \Gamma,\\
\frac{\partial q}{\partial \boldsymbol{n}} &= 0 && \text{on } \Gamma_W,\\
\boldsymbol{v} &= 0 && \text{on } \Gamma_D,\\
\sigma(\boldsymbol{v})\boldsymbol{n} &= 0 && \text{on } \Gamma_N.
\end{aligned}$$

4.4 Shape-Lagrangian functional

Given $\boldsymbol{\theta} \in \mathcal{D}^k(\mathfrak{D}, \mathbb{R}^3), k \geq 1$, we define the flows $\Omega_F^t := \Phi_t(\Omega_F)$ and $\Omega_S^t := \Phi_t(\Omega_S)$ as in Section 4.1. For the perturbed domains Ω_F^t, Ω_S^t, the objective function is given by

$$J(\Omega_F^t, \Omega_S^t) = \mathcal{L}\big((\Omega_F^t, \Omega_S^t), (p_t, \boldsymbol{u}_t), (\mathfrak{q}, \mathfrak{v})\big),$$

where $(p_t, \boldsymbol{u}_t) \in \mathcal{H}_t$ is the solution of (2.2), in which $\mathcal{H}$ is replaced by $\mathcal{H}_t := H^1(\Omega_F^t) \times (H^1_{\Gamma_D^t}(\Omega_S^t))^3$. We also introduce the notations $\Gamma^t := \Phi_t(\Gamma), \Gamma_N^t := \Phi_t(\Gamma_N), \Gamma_D^t := \Phi_t(\Gamma_D)$. The main difficulty in differentiating $J(\Omega_F^t, \Omega_S^t)$ with respect to t is that p_t and $\boldsymbol{u}_t$ live in function spaces that depend on t. Following the general procedure described in Section 4.2, this issue can be solved by using the parameterization

$$H^1(\Omega_F^t) = \{\mathfrak{p} \circ \Phi_t^{-1} : \mathfrak{p} \in \mathrm{H}^1(\Omega_F)\} \quad \text{and} \quad \left(H^1_{\Gamma_D^t}(\Omega_S^t)\right)^3 = \{\mathfrak{u} \circ \Phi_t^{-1} : \mathfrak{u} \in \left(\mathrm{H}^1_{\Gamma_D}(\Omega_S)\right)^3\}.$$

Then, for $(\mathfrak{p}, \mathfrak{u}), (\mathfrak{q}, \mathfrak{v}) \in \mathcal{H}$ we define the shape-Lagrangian

$$G(t, (\mathfrak{p}, \mathfrak{u}), (\mathfrak{q}, \mathfrak{v})) := \mathcal{L}\big((\Omega_F^t, \Omega_S^t), (\mathfrak{p} \circ \Phi_t^{-1}, \mathfrak{u} \circ \Phi_t^{-1}), (\mathfrak{q} \circ \Phi_t^{-1}, \mathfrak{v} \circ \Phi_t^{-1})\big). \tag{4.15}$$

This yields the formula

$$\begin{aligned}
G(t, (\mathfrak{p}, \mathfrak{u}), (\mathfrak{q}, \mathfrak{v})) = &\int_{\Omega_F^t} \kappa |\mathfrak{p} \circ \Phi_t^{-1} - p_d|^2 \, \mathrm{d}x\\
&+ \Re\left(\int_{\Omega_F^t} \nabla(\mathfrak{p} \circ \Phi_t^{-1}) \cdot \nabla\left(\overline{\mathfrak{q}} \circ \Phi_t^{-1}\right) \mathrm{d}x - \frac{\omega^2}{c^2} \int_{\Omega_F^t} (\mathfrak{p} \circ \Phi_t^{-1}) \left(\overline{\mathfrak{q}} \circ \Phi_t^{-1}\right) \mathrm{d}x \right.\\
&- \rho_F \omega^2 \int_{\Gamma^t} (\mathfrak{u} \circ \Phi_t^{-1} \cdot \boldsymbol{n}_t) \overline{\mathfrak{q}} \circ \Phi_t^{-1} \, \mathrm{d}\sigma - \rho_F \omega^2 \int_{\Gamma^t} \mathfrak{p} \circ \Phi_t^{-1} \left(\boldsymbol{n}_t \cdot \overline{\mathfrak{v}} \circ \Phi_t^{-1}\right) \mathrm{d}\sigma\\
&+ \rho_F \omega^2 \int_{\Omega_S^t} \sigma(\mathfrak{u} \circ \Phi_t^{-1}) : \varepsilon\left(\overline{\mathfrak{v}} \circ \Phi_t^{-1}\right) \mathrm{d}x + \rho_F \rho_S \omega^4 \int_{\Omega_S^t} \mathfrak{u} \circ \Phi_t^{-1} \cdot \overline{\mathfrak{v}} \circ \Phi_t^{-1} \, \mathrm{d}x\\
&\left. - \rho_F \omega^2 \int_{\Omega_S^t} \boldsymbol{f} \cdot \left(\overline{\mathfrak{v}} \circ \Phi_t^{-1}\right) \mathrm{d}x - \rho_F \omega^2 \int_{\Gamma_N^t} \boldsymbol{g} \cdot \left(\overline{\mathfrak{v}} \circ \Phi_t^{-1}\right) \mathrm{d}\sigma \right).
\end{aligned}$$

Here, $\boldsymbol{n}_t$ denotes the outward unit normal to Ω_S^t. Using the change of variables $t \mapsto \boldsymbol{\Phi}_t$ and (4.2)–(4.5), we obtain

$$\begin{aligned} G(t,(\mathfrak{p},\mathfrak{u}),(\mathfrak{q},\mathfrak{v})) &= \int_{\Omega_F} j(t)\kappa\circ\Phi_t|\mathfrak{p}-p_d\circ\Phi_t|^2\,\mathrm{d}x \\ &+ \mathrm{Re}\Big(\int_{\Omega_F}\boldsymbol{A}(t)\nabla\mathfrak{p}\cdot\nabla\overline{\mathfrak{q}}\,\mathrm{d}x - \frac{\omega^2}{c^2}\int_{\Omega_F} j(t)\mathfrak{p}\overline{\mathfrak{q}}\,\mathrm{d}x - \rho_F\omega^2\int_\Gamma(\mathfrak{u}\cdot\boldsymbol{B}(t)\boldsymbol{n})\overline{\mathfrak{q}}\,\mathrm{d}\sigma \\ &- \rho_F\omega^2\int_\Gamma\mathfrak{p}(\boldsymbol{B}(t)\boldsymbol{n}\cdot\overline{\mathfrak{v}})\,\mathrm{d}\sigma + \rho_F\omega^2\int_{\Omega_S} j(t)\sigma^t(\mathfrak{u}):\varepsilon^t\left(\overline{\mathfrak{v}}\right)\mathrm{d}x \\ &- \rho_F\rho_S\omega^4\int_{\Omega_S} j(t)\mathfrak{u}\cdot\overline{\mathfrak{v}}\mathrm{d}x - \rho_F\omega^2\int_{\Omega_S} j(t)(\boldsymbol{f}\circ\Phi_t)\cdot\overline{\mathfrak{v}}\,\mathrm{d}x - \rho_F\omega^2\int_{\Gamma_N} j_\Gamma(t)(\boldsymbol{g}\circ\Phi_t)\cdot\overline{\mathfrak{v}}\,\mathrm{d}\sigma\Big), \end{aligned} \tag{4.16}$$

where we have used, for $t\in[0,\tau]$, the notations

$$\begin{aligned} &j(t) := |\det D\Phi_t|, \qquad \boldsymbol{A}(t) := j(t)(D\Phi_t)^{-1}(D\Phi_t)^{-T}, \qquad \boldsymbol{B}(t) := j(t)(D\Phi_t)^{-T}, \\ &\sigma^t(\mathfrak{u}) := \lambda\ \mathrm{trace}\ \varepsilon^t(\mathfrak{u})\boldsymbol{I} + 2\mu\varepsilon^t(\mathfrak{u}), \qquad \varepsilon^t(\mathfrak{u}) := \frac{1}{2}\left(D\mathfrak{u}(D\Phi_t)^{-1} + (D\Phi_t)^{-T}D\mathfrak{u}^T\right). \end{aligned} \tag{4.17}$$

Note that the expression of $\boldsymbol{B}(t)$ follows from the following calculation, using Lemma 4.3,

$$\boldsymbol{B}(t)\boldsymbol{n} = j_\Gamma(t)\boldsymbol{n}_t\circ\Phi_t = j(t)|(D\Phi_t)^{-T}\boldsymbol{n}|\frac{(D\Phi_t)^{-T}\boldsymbol{n}}{\left|(D\Phi_t)^{-T}\boldsymbol{n}\right|} = j(t)(D\Phi_t)^{-T}\boldsymbol{n}.$$

4.5 State equation

In order to compute the shape derivative we apply Theorem 4.8, for which we need to verify first that the state equation (4.7) has a unique solution for each $t\in[0,\tau]$. Let us introduce $(p^t,\boldsymbol{u}^t)=(p_t\circ\Phi_t,\boldsymbol{u}_t\circ\Phi_t)\in\mathcal{H}$, which corresponds to the solution $\mathfrak{e}^t$ of (4.7), while $(\widehat{q},\widehat{\boldsymbol{v}})\in\mathcal{H}$ corresponds to the test function $\widehat{\psi}$ in (4.7). Differentiating (4.16) with respect to $(\mathfrak{q},\mathfrak{v})\in\mathcal{H}$ in direction $(\widehat{q},\widehat{\boldsymbol{v}})$ at $(\mathfrak{p},\mathfrak{u})=(p^t,\boldsymbol{u}^t)$, we obtain the variational formulation (4.7). Note that although (4.16) contains only the real part of the PDE, by choosing first purely real and then purely imaginary test functions we can recover both the real and the complex parts of the PDE; see Hintermüller *et al.* (2015) for details. Thus (4.7) corresponds to the variational equation

$$B^t\left((p^t,\boldsymbol{u}^t),\left(\widehat{q},\widehat{\boldsymbol{v}}\right)\right) = L^t\left(\widehat{q},\widehat{\boldsymbol{v}}\right) \quad \text{for all } \left(\widehat{q},\widehat{\boldsymbol{v}}\right)\in\mathcal{H}, \tag{4.18}$$

where

$$\begin{aligned} B^t((\mathfrak{p},\mathfrak{u}),(\mathfrak{q},\mathfrak{v})) := {} & B_F^t(\mathfrak{p},\mathfrak{q}) - \rho_F\omega^2 B_{FS}^t((\mathfrak{p},\mathfrak{u}),(\mathfrak{q},\mathfrak{v})) - \rho_F\omega^2 B_{FS}^{*,t}((\mathfrak{p},\mathfrak{u}),(\mathfrak{q},\mathfrak{v})) \\ & + \rho_F\omega^2 B_S^t(\mathfrak{u},\mathfrak{v}), \end{aligned} \tag{4.19}$$

with

$$\begin{aligned} B_F^t(\mathfrak{p},\mathfrak{q}) &:= \int_{\Omega_F}\boldsymbol{A}(t)\nabla\mathfrak{p}\cdot\nabla\overline{\mathfrak{q}}\,\mathrm{d}x - \frac{\omega^2}{c^2}\int_{\Omega_F} j(t)\mathfrak{p}\overline{\mathfrak{q}}\,\mathrm{d}x, \\ B_{FS}^t((\mathfrak{p},\mathfrak{u}),(\mathfrak{q},\mathfrak{v})) &:= \int_\Gamma(\mathfrak{u}\cdot\boldsymbol{B}(t)\boldsymbol{n})\overline{\mathfrak{q}}\,\mathrm{d}\sigma, \\ B_{FS}^{*,t}((\mathfrak{p},\mathfrak{u}),(\mathfrak{q},\mathfrak{v})) &:= \overline{B_{FS}((\mathfrak{q},\mathfrak{v}),(\mathfrak{p},\mathfrak{u}))} := \int_\Gamma\mathfrak{p}\left(\boldsymbol{B}(t)\boldsymbol{n}\cdot\overline{\mathfrak{v}}\right)\mathrm{d}\sigma, \\ B_S^t(\mathfrak{u},\mathfrak{v}) &:= \int_{\Omega_S} j(t)\sigma^t(\mathfrak{u}):\varepsilon^t\left(\overline{\mathfrak{v}}\right)\mathrm{d}x - \rho_S\omega^2\int_{\Omega_S} j(t)\mathfrak{u}\cdot\overline{\mathfrak{v}}\,\mathrm{d}x, \end{aligned}$$

and

$$L^t((\mathfrak{q},\mathfrak{v})) = \rho_F\omega^2\left(\int_{\Omega_S} j(t)(\boldsymbol{f}\circ\Phi_t)\cdot\overline{\mathfrak{v}}\,\mathrm{d}x + \int_{\Gamma_N} j_\Gamma(t)(\boldsymbol{g}\circ\Phi_t)\cdot\overline{\mathfrak{v}}\,\mathrm{d}\sigma\right).$$

Note that we have $j(0) = 1$, $\boldsymbol{A}(0) = \boldsymbol{B}(0) = Id$, and consequently (4.18) at $t = 0$ corresponds to the weak formulation (2.2). The following lemma states that, with the assumptions made, the difference between $(p^t, \boldsymbol{u}^t)$ and $(p, \boldsymbol{u})$ is of order t.

Lemma 4.9. *Assume that ω is not an eigenfrequency of the state equation (2.2). Then, there exists $\tau > 0$ and $C > 0$ such that (4.18) has a unique solution $(p^t, \boldsymbol{u}^t)$ for all $t \in [0, \tau]$ and it holds*

$$\|(p^t, \boldsymbol{u}^t)\|_{\mathcal{H}} \le C\left(\|\boldsymbol{f}\|_{(L^2(\Omega_S))^3} + \|\boldsymbol{g}\|_{(L^2(\Gamma_N))^3}\right),\ \|(p^t, \boldsymbol{u}^t) - (p, \boldsymbol{u})\|_{\mathcal{H}} \le C\,t. \tag{4.20}$$

Proof. Since by assumption $D\boldsymbol{\theta}$ is bounded in $\mathfrak{D}$, we find with the fix point form of (4.1)

$$\boldsymbol{x}(t) - \boldsymbol{x}_0 = \int_0^t \boldsymbol{\theta}(\boldsymbol{x}(s))ds$$

and with the Picard–Lindelöf theorem that for $\boldsymbol{\Phi}_t = \boldsymbol{x}(t)$ it holds

$$\sup_{\mathfrak{D}}\|D\Phi_t - \mathrm{Id}\| \le C\,t, \quad \forall t \in (0,\tau)$$

for some $\tau > 0$ small enough, where $C > 0$ denotes a generic constant independent of t. Hence, we find that

$$\sup_{\mathfrak{D}}|j(t) - 1| + \sup_{\mathfrak{D}}\|\boldsymbol{A}(t) - \mathrm{Id}\| + \sup_{\mathfrak{D}}\|\boldsymbol{B}(t) - \mathrm{Id}\| \le C\,t, \tag{4.21}$$

where we have used properties of geometric series to estimate the last two terms. Proceeding in a similar way as in the proof of Theorem 3.1, we define operators $A^t, M^t : \mathcal{H} \to \mathcal{H}$ and $F^t \in \mathcal{H}$ such that (4.18) can be written as

$$\left(A^t - (\omega^2 + 1)M^t\right)(p^t, \boldsymbol{u}^t) = F^t, \tag{4.22}$$

where $A^t \to A, M^t \to M$ and $F^t \to F$ converge strongly in the respective norms when $t \to 0$ due to the estimates (4.21). The equation is well-posed by the Fredholm–Riesz–Schauder theory (Sauter and Schwab, 2011, Sec. 2.1.4) except for countably many eigenvalues λ^t of the compact operator $T^t := (A^t)^{-1}M^t$. As $T^t \to T$ when $t \to 0$ each eigenvalue λ^t tends to an eigenvalue of T when $t \to 0$ (Kato, 1995, Chap. IV). More precisely, if λ is an eigenvalue of T of multiplicity m then m eigenvalues of T^t tend to λ as well as the respective generalized eigenspace.
As ω is assumed not to be an eigenfrequency of the state equation, there exists a neighborhood $(0, \tau)$ of 0 in which ω is not an eigenfrequency of the perturbed problem and (4.18) provides a unique solution. Moreover, using (3.2) and (4.22), the difference $(p^t - p, \boldsymbol{u}^t - \boldsymbol{u})$ satisfies

$$\begin{aligned}\left(A - (\omega^2+1)M\right)(p^t - p, \boldsymbol{u}^t - \boldsymbol{u}) &= \left(F^t - F\right) + \left(A - A^t - (\omega^2+1)(M - M^t)\right)(p^t, \boldsymbol{u}^t)\\ &=: G^t \in \mathcal{H}\end{aligned}$$

where it holds $\|G^t\|_{\mathcal{H}} \le C\,t$ due to (4.21). This implies the second inequality in (4.20), and the proof is complete.

4.6 Calculation of the distributed shape derivative

In this section, we apply Theorem 4.8 to compute the distributed shape derivative of $J(\Omega_F^t, \Omega_S^t)$.

Theorem 4.10. *Assume that ω is not an eigenfrequency of the state equation (2.2), whose solution is denoted by $(p, \boldsymbol{u}) \in \mathcal{H}$. Then, the system of the adjoint equation (4.14) is well-posed and possesses a unique solution $(q, \boldsymbol{v}) \in \mathcal{H}$. Also, J is shape differentiable and its distributed shape derivative in direction $\boldsymbol{\theta} \in \mathcal{D}^k(\mathfrak{D}, \mathbb{R}^3)$, $k \geq 1$ is given by*

$$
\begin{aligned}
dJ(\Omega_F, \Omega_S; \boldsymbol{\theta}) = \int_{\Omega_F} & \kappa |p - p_d|^2 \operatorname{div} \boldsymbol{\theta} + |p - p_d|^2 \nabla \kappa \cdot \boldsymbol{\theta} - 2\kappa \operatorname{Re}\Big(\big(\overline{p} - \overline{p}_d\big) \nabla p_d \Big) \cdot \boldsymbol{\theta} \, \mathrm{d}x \\
& + \operatorname{Re}\Bigg(\int_{\Omega_F} \boldsymbol{A}'(0) \nabla p \cdot \nabla \overline{q} - \frac{\omega^2}{c^2} p \overline{q} \operatorname{div} \boldsymbol{\theta} \, \mathrm{d}x - \rho_F \omega^2 \int_\Gamma (\boldsymbol{u} \cdot \boldsymbol{B}'(0) \boldsymbol{n}) \overline{q} + \Big(\overline{\boldsymbol{v}} \cdot \boldsymbol{B}'(0) \boldsymbol{n} \Big) p \, \mathrm{d}\sigma \\
& + \rho_F \omega^2 \int_{\Omega_S} (\operatorname{div} \boldsymbol{\theta}) \sigma(\boldsymbol{u}) : \varepsilon\Big(\overline{\boldsymbol{v}}\Big) - \sigma'_{\boldsymbol{\theta}}(\boldsymbol{u}) : \varepsilon\Big(\overline{\boldsymbol{v}}\Big) - \sigma(\boldsymbol{u}) : \varepsilon'_{\boldsymbol{\theta}}\Big(\overline{\boldsymbol{v}}\Big) \, \mathrm{d}x \\
& - \rho_F \rho_S \omega^4 \int_{\Omega_S} \operatorname{div} \boldsymbol{\theta} \, \boldsymbol{u} \cdot \overline{\boldsymbol{v}} \, \mathrm{d}x - \rho_F \omega^2 \int_{\Omega_S} (D\boldsymbol{f}\boldsymbol{\theta}) \cdot \overline{\boldsymbol{v}} + \operatorname{div} \boldsymbol{\theta} \, \boldsymbol{f} \cdot \overline{\boldsymbol{v}} \, \mathrm{d}x \\
& - \rho_F \omega^2 \int_{\Gamma_N} (D\boldsymbol{g}\boldsymbol{\theta}) \cdot \overline{\boldsymbol{v}} + j'_\Gamma(0) \, \boldsymbol{g} \cdot \overline{\boldsymbol{v}} \, \mathrm{d}\sigma \Bigg),
\end{aligned}
\tag{4.23}
$$

with the notations

$$
\begin{aligned}
j'(0) &= \operatorname{div} \boldsymbol{\theta}, & j'_\Gamma(0) &= \operatorname{div} \boldsymbol{\theta} - (D\boldsymbol{\theta}\boldsymbol{n}) \cdot \boldsymbol{n} = \operatorname{div}_\Gamma \boldsymbol{\theta}, \\
\boldsymbol{A}'(0) &= \operatorname{div}(\boldsymbol{\theta}) \boldsymbol{I} - D\boldsymbol{\theta} - D\boldsymbol{\theta}^T, & \boldsymbol{B}'(0) &= \operatorname{div}(\boldsymbol{\theta}) \boldsymbol{I} - D\boldsymbol{\theta}^T, \\
\sigma'_{\boldsymbol{\theta}}(\boldsymbol{u}) &= \lambda \operatorname{trace} \varepsilon'_{\boldsymbol{\theta}}(\boldsymbol{u}) \boldsymbol{I} + 2\mu \varepsilon'_{\boldsymbol{\theta}}(\boldsymbol{u}), & \varepsilon'_{\boldsymbol{\theta}}(\boldsymbol{u}) &= \frac{1}{2} \Big(D\boldsymbol{u} D\boldsymbol{\theta} + D\boldsymbol{\theta}^T D\boldsymbol{u}^T \Big).
\end{aligned}
$$

Proof. Following the notations of Section 4.2, we have $E = E_1 \times E_2$ and $F = F_1 \times F_2$, with $E_1 = F_1 = H^1(\Omega_F)$ and $E_2 = F_2 = \left(H^1_{\Gamma_D}(\Omega_S)\right)^3$. The proof consists in verifying the assumptions of Theorem 4.8. Note that Assumption 4.6 is straightforwardly satisfied, indeed (1) and (2) are satisfied since G is affine with respect to $\mathfrak{q}$, $\mathfrak{v}$ and $\mathfrak{u}$, and depends quadratically on $\mathfrak{p}$. Then, by Lemma 4.9 the formulation (4.18) has a unique solution $(p^t, \boldsymbol{u}^t)$ for all $t \in [0, \tau]$, for some $\tau > 0$.

Existence of solution to the averaged adjoint equation. Now we prove the uniqueness of solution for the averaged adjoint equation (4.8). To compute the equation, we take the derivative of (4.16) with respect to $(\mathfrak{p}, \mathfrak{u})$ in direction $(\widehat{p}, \widehat{\boldsymbol{u}})$ at $s\mathfrak{e}^t + (1-s)\mathfrak{e}^0$ with $\mathfrak{e}^t = (p^t, \boldsymbol{u}^t)$ and $\mathfrak{f}^t = (q^t, \boldsymbol{v}^t)$. Note that in (4.16), all terms are either linear in $(\mathfrak{p}, \mathfrak{u})$ or independent of $(\mathfrak{p}, \mathfrak{u})$, except for the first integral, which depends quadratically on $\mathfrak{p}$. This is due to the fact that we work with a linear PDE. Therefore, the integral with respect to s in (4.9) only affects the derivative of the term depending quadratically on $\mathfrak{p}$, which simplifies the equation. Choosing first purely real and then purely imaginary test functions, we obtain the following equation for the averaged adjoint $\mathfrak{f}^t = (q^t, \boldsymbol{v}^t)$:

$$\int_{\Omega_F} \boldsymbol{A}(t)\nabla\widehat{p}\cdot\nabla\overline{q^t}\,\mathrm{d}x - \frac{\omega^2}{c^2}\int_{\Omega_F} j(t)\widehat{p}\overline{q^t}\,\mathrm{d}x - \rho_F\omega^2\int_\Gamma \left(\widehat{\boldsymbol{u}}\cdot\boldsymbol{B}(t)\boldsymbol{n}\right)\overline{q^t}\,\mathrm{d}\sigma - \rho_F\omega^2\int_\Gamma \widehat{p}\left(\boldsymbol{B}(t)\boldsymbol{n}\cdot\overline{\boldsymbol{v}^t}\right)\mathrm{d}\sigma$$
$$+\rho_F\omega^2\int_{\Omega_S} j(t)\sigma^t\left(\widehat{\boldsymbol{u}}\right) : \varepsilon^t\left(\overline{\boldsymbol{v}^t}\right)\mathrm{d}x - \rho_F\rho_S\omega^4\int_{\Omega_S} j(t)\widehat{\boldsymbol{u}}\cdot\overline{\boldsymbol{v}^t}\,\mathrm{d}x$$
$$= -\int_0^1\int_{\Omega_F} 2j(t)\kappa\circ\Phi_t\left(s\overline{p^t} + (1-s)\overline{p} - \overline{p_d}\circ\Phi_t\right)\widehat{p}\,dxds$$
$$= -\int_{\Omega_F} j(t)\kappa\circ\Phi_t\left(\overline{p^t} + \overline{p} - 2\overline{p_d}\circ\Phi_t\right)\widehat{p}\,\mathrm{d}x \qquad \text{for all } \left(\widehat{p},\widehat{\boldsymbol{u}}\right)\in\mathcal{H}. \tag{4.24}$$

now, we observe that $\boldsymbol{A}(t) = \boldsymbol{A}(t)^{\mathsf{T}}$, $\overline{\boldsymbol{A}(t)} = \boldsymbol{A}(t)$ and $\boldsymbol{B}(t) = \boldsymbol{B}(t)^{\mathsf{T}}$, $\overline{\boldsymbol{B}(t)} = \boldsymbol{B}(t)$. We also have

$$\overline{\sigma^t\left(\widehat{\boldsymbol{u}}\right) : \varepsilon^t\left(\overline{\boldsymbol{v}^t}\right)} = \sigma^t\left(\overline{\widehat{\boldsymbol{u}}}\right) : \varepsilon^t\left(\boldsymbol{v}^t\right) = \varepsilon^t\left(\overline{\widehat{\boldsymbol{u}}}\right) : \sigma^t\left(\boldsymbol{v}^t\right).$$

using these properties and taking the complex conjugate of (4.24), we obtain the equation

$$\int_{\Omega_F} \boldsymbol{A}(t)\nabla q^t\cdot\nabla\overline{\widehat{p}}\,\mathrm{d}x - \frac{\omega^2}{c^2}\int_{\Omega_F} j(t)q^t\overline{\widehat{p}}\,\mathrm{d}x - \rho_F\omega^2\int_\Gamma \left(\overline{\widehat{\boldsymbol{u}}}\cdot\boldsymbol{B}(t)\boldsymbol{n}\right)q^t\,\mathrm{d}\sigma - \rho_F\omega^2\int_\Gamma \overline{\widehat{p}}\left(\boldsymbol{B}(t)\boldsymbol{n}\cdot\boldsymbol{v}^t\right)\mathrm{d}\sigma$$
$$+\rho_F\omega^2\int_{\Omega_S} j(t)\sigma^t\left(\boldsymbol{v}^t\right) : \varepsilon^t\left(\overline{\widehat{\boldsymbol{u}}}\right)\mathrm{d}x - \rho_F\rho_S\omega^4\int_{\Omega_S} j(t)\overline{\widehat{\boldsymbol{u}}}\cdot\boldsymbol{v}^t\,\mathrm{d}x$$
$$= -\int_{\Omega_F} j(t)\kappa\circ\Phi_t\left(p^t + p - 2p_d\circ\Phi_t\right)\overline{\widehat{p}}\,\mathrm{d}x \qquad \text{for all } \left(\widehat{p},\widehat{\boldsymbol{u}}\right)\in\mathcal{H}. \tag{4.25}$$

Equation (4.25) can be written as

$$B^t\left(\left(q^t,\boldsymbol{v}^t\right),\left(\widehat{p},\widehat{\boldsymbol{u}}\right)\right) = -\int_{\Omega_F} j(t)\kappa\circ\Phi_t\left(p^t + p - 2p_d\circ\Phi_t\right)\overline{\widehat{p}}\,\mathrm{d}x \qquad \text{for all } \left(\widehat{p},\widehat{\boldsymbol{u}}\right)\in\mathcal{H}.$$

where B^t is defined in the perturbed state equation (4.18). In view of (4.20) we have that $\|(p^t,\boldsymbol{u}^t)\|_{\mathcal{H}}$ is uniformly bounded for $t\in[0,\tau]$. Thus, since we assume that ω is not an eigenfrequency of the state equation (2.2), we can apply Lemma 4.9 to prove that the averaged adjoint (4.25) has a unique solution $(q^t,\boldsymbol{v}^t)$ for each $t\in[0,\tau]$.

Also, proceeding as in the proof of Lemma 4.9, we obtain the estimates.

$$\left\|\left(q^t,\boldsymbol{v}^t\right) - (q,\boldsymbol{v})\right\|_{\mathcal{H}} \leq C\,t, \tag{4.26}$$

$$\left\|\left(q^t,\boldsymbol{v}^t\right)\right\|_{\mathcal{H}} \leq C, \tag{4.27}$$

for all $t\in[0,\tau]$ where C is independent on t.

Verification of Assumption 4.7. To compute $\partial_t G(t, \mathfrak{e}^0, \psi)$, we differentiate (4.16) with respect to t at $(\mathfrak{p}, \mathfrak{u}) = (p, \boldsymbol{u})$ with the notations $\mathfrak{e}^0 = (p, \boldsymbol{u})$ and $\psi = (\mathfrak{q}, \mathfrak{v})$. Since $\boldsymbol{\Phi}_t$ is continuously differentiable with respect to $t \in [0, \tau]$, $(p, \boldsymbol{u}), (\mathfrak{q}, \mathfrak{v}) \in \mathcal{H}$ and $\boldsymbol{f} \in H^1(\Omega_S)$, $\boldsymbol{g} \in H^1(\Gamma_N)$ then all terms in the derivative below are well-defined. Thus, the derivative $\partial_t G(t, \mathfrak{e}^0, \psi)$ exists for all $t \in 0, \tau]$ and $\psi \in F$, and we obtain

$$\begin{aligned}
\partial_t G(t, (p, \boldsymbol{u}), (\mathfrak{q}, \mathfrak{v})) = & \int_{\Omega_F} j'(t) \kappa \circ \Phi_t |p - p_d \circ \Phi_t|^2 \, \mathrm{d}x + \int_{\Omega_F} j(t) \nabla \kappa \cdot \boldsymbol{\theta}_t |p - p_d \circ \Phi_t|^2 \, \mathrm{d}x \\
& - 2 \int_{\Omega_F} j(t) \kappa \circ \Phi_t \mathrm{Re}\left(\left(\overline{p} - \overline{p}_d \circ \Phi_t \right) \nabla p_d \cdot \boldsymbol{\theta}_t \right) \mathrm{d}x \\
& + \mathrm{Re}\left(\int_{\Omega_F} \boldsymbol{A}'(t) \nabla p \cdot \nabla \overline{\mathfrak{q}} \, \mathrm{d}x - \frac{\omega^2}{c^2} \int_{\Omega_F} j'(t) p \overline{\mathfrak{q}} \, \mathrm{d}x \right. \\
& - \rho_F \omega^2 \int_{\Gamma} (\boldsymbol{u} \cdot \boldsymbol{B}'(t) \boldsymbol{n}) \overline{\mathfrak{q}} + p \left(\boldsymbol{B}'(t) \boldsymbol{n} \cdot \overline{\mathfrak{v}} \right) \mathrm{d}\sigma \\
& + \rho_F \omega^2 \int_{\Omega_S} j'(t) \sigma^t(\boldsymbol{u}) : \varepsilon^t \left(\overline{\mathfrak{v}} \right) - j(t) \sigma'_{\boldsymbol{\theta},t}(\boldsymbol{u}) : \varepsilon^t \left(\overline{\mathfrak{v}} \right) \mathrm{d}x \\
& - \rho_F \omega^2 \int_{\Omega_S} j(t) \sigma^t(\boldsymbol{u}) : \varepsilon'_{\boldsymbol{\theta},t} \left(\overline{\mathfrak{v}} \right) \mathrm{d}x - \rho_F \rho_S \omega^4 \int_{\Omega_S} j'(t) \boldsymbol{u} \cdot \overline{\mathfrak{v}} \, \mathrm{d}x \\
& - \rho_F \omega^2 \int_{\Omega_S} j(t) (D\boldsymbol{f} \boldsymbol{\theta}_t) \cdot \overline{\mathfrak{v}} + j'(t) (\boldsymbol{f} \circ \Phi_t) \cdot \overline{\mathfrak{v}} \, \mathrm{d}x \\
& \left. - \rho_F \omega^2 \int_{\Gamma_N} j(t) (D\boldsymbol{g} \boldsymbol{\theta}_t) \cdot \overline{\mathfrak{v}} + j'_{\Gamma}(t) (\boldsymbol{g} \circ \Phi_t) \cdot \overline{\mathfrak{v}} \, \mathrm{d}\sigma \right).
\end{aligned} \tag{4.28}$$

here, we have used $\boldsymbol{\theta}_t := \boldsymbol{\theta} \circ \Phi_t = \frac{\partial}{\partial t} \Phi_t$, which is a consequence of the definition (4.1) of $\boldsymbol{\Phi}_t$, and the notations

$$\begin{aligned}
\sigma'_{\boldsymbol{\theta},t}(\boldsymbol{u}) &:= \lambda \, \mathrm{trace} \, \varepsilon'_{\boldsymbol{\theta},t}(\boldsymbol{u}) \boldsymbol{I} + 2\mu \varepsilon'_{\boldsymbol{\theta},t}(\boldsymbol{u}), \\
\varepsilon'_{\boldsymbol{\theta},t}(\boldsymbol{u}) &:= \frac{1}{2} \left(D\boldsymbol{u} (D\Phi_t)^{-1} D\boldsymbol{\theta}_t (D\Phi_t)^{-1} + (D\Phi_t)^{-T} D\boldsymbol{\theta}_t^T (D\Phi_t)^{-T} D\boldsymbol{u}^T \right).
\end{aligned}$$

For $t \in [0, \tau]$ we have the expansion

$$G(t, (p, \boldsymbol{u}), (\mathfrak{q}, \mathfrak{v})) = G(0, (p, \boldsymbol{u}), (\mathfrak{q}, \mathfrak{v})) + t \partial_t G(\xi(t, (\mathfrak{q}, \mathfrak{v})), (p, \boldsymbol{u}), (\mathfrak{q}, \mathfrak{v})) \tag{4.29}$$

for some $0 \leq \xi(t, (\mathfrak{q}, \mathfrak{v})) \leq t$. Then, choosing $(\mathfrak{q}, \mathfrak{v}) = (q^t, \boldsymbol{v}^t)$ we get

$$\begin{aligned}
& \frac{G(t, (p, \boldsymbol{u}), (q^t, \boldsymbol{v}^t)) - G(0, (p, \boldsymbol{u}), (q^t, \boldsymbol{v}^t))}{t} - \partial_t G(0, (p, \boldsymbol{u}), (q, \boldsymbol{v})) \\
& \quad = \partial_t G(\xi(t, (q^t, \boldsymbol{v}^t)), (p, \boldsymbol{u}), (q^t, \boldsymbol{v}^t)) - \partial_t G(0, (p, \boldsymbol{u}), (q, \boldsymbol{v})).
\end{aligned}$$

Thus, in order to prove Assumption 4.7, it is enough to prove that $(s, t) \mapsto \partial_t G(s, (p, \boldsymbol{u}), (q^t, \mathfrak{v}^t))$ is continuous for $(s, t) \in [0, \tau] \times [0, \tau]$. The mappings $t \mapsto j(t)$ and $t \mapsto D\boldsymbol{\Phi}_t$ are continuously differentiable (Sokolowski and Zolesio, 1992, Proposition 2.44) and we have

$$\frac{\partial}{\partial t} j(t) = j(t) \mathrm{div} \, \boldsymbol{\theta}_t \circ \Phi_t$$

and

$$\frac{\partial}{\partial t} D\Phi_t = D(\boldsymbol{\theta} \circ \Phi_t) = D\boldsymbol{\theta} \circ \Phi_t D\Phi_t.$$

Thus, the mappings $t \mapsto j'(t), t \mapsto \boldsymbol{A}'(t), t \mapsto \boldsymbol{B}'(t), t \mapsto j'_\Gamma(t)$ and $(D\Phi_t)^{-1} D\boldsymbol{\theta}_t$ are continuous and uniformly bounded on $[0, \tau]$. Using the estimates (4.20) (4.26), (4.27) and expression (4.28) we obtain that

$$(s,t) \mapsto \partial_t G\big(s, (p, \boldsymbol{u}), \big(\mathfrak{q}^t, \mathfrak{v}^t\big)\big)$$

is uniformly bounded and continuous on $[0, \tau] \times [0, \tau]$, which proves Assumption 4.7.

Now all assumptions of Theorem 4.8 are satisfied. Taking $t = 0$ and $(\mathfrak{q}, \mathfrak{v}) = (q, \boldsymbol{v})$ in (4.28), we obtain the distributed shape derivative (4.23).

Proposition 4.11. Assume that the assumptions of Theorem 4.10 are satisfied. The tensor form of the distributed shape derivative of J in direction $\boldsymbol{\theta} \in \mathcal{D}^k(\mathfrak{D}, \mathbb{R}^3)$, $k \geq 1$ is given by

$$\begin{aligned} dJ(\Omega_F, \Omega_S; \boldsymbol{\theta}) = &\int_{\Omega_F} \mathbf{S}_1^F : D\boldsymbol{\theta} + \mathbf{S}_0^F \cdot \boldsymbol{\theta} \, \mathrm{d}x + \int_{\Omega_S} \mathbf{S}_1^S : D\boldsymbol{\theta} + \mathbf{S}_0^S \cdot \boldsymbol{\theta} \, \mathrm{d}x \\ &+ \int_\Gamma \mathfrak{S}_1 : D_\Gamma \boldsymbol{\theta} \, \mathrm{d}\sigma + \int_{\Gamma_N} \mathfrak{S}_1^N : D_\Gamma \boldsymbol{\theta} + \mathfrak{S}_0^N \cdot \boldsymbol{\theta} \, \mathrm{d}\sigma, \end{aligned} \tag{4.30}$$

with

$$\mathbf{S}_1^F = \left(\kappa |p - p_d|^2 + \mathrm{Re}\left(\nabla p \cdot \nabla \overline{q} - \frac{\omega^2}{c^2} p \overline{q}\right)\right) \boldsymbol{I} - \mathrm{Re}(2 \nabla p \odot \nabla \overline{q})$$

$$\mathbf{S}_0^F = |p - p_d|^2 \nabla \kappa - 2\kappa \mathrm{Re}\Big(\big(\overline{p} - \overline{p}_d\big) \nabla p_d\Big)$$

$$\mathbf{S}_1^S = \mathrm{Re}\Big(\rho_F \omega^2 \sigma(\boldsymbol{u}) : \varepsilon\big(\overline{\boldsymbol{v}}\big) - \rho_F \rho_S \omega^4 \boldsymbol{u} \cdot \overline{\boldsymbol{v}} - \rho_F \omega^2 \boldsymbol{f} \cdot \overline{\boldsymbol{v}}\Big) \boldsymbol{I} - \mathrm{Re}\Big(\rho_F \omega^2 \big(D\overline{\boldsymbol{v}}^\mathsf{T} \sigma(\boldsymbol{u}) + D\boldsymbol{u}^\mathsf{T} \sigma\big(\overline{\boldsymbol{v}}\big)\big)\Big)$$

$$\mathbf{S}_0^S = -\mathrm{Re}\big(\rho_F \omega^2 D\boldsymbol{f}^\mathsf{T} \overline{\boldsymbol{v}}\big)$$

$$\mathfrak{S}_1^N = -\mathrm{Re}\big(\rho_F \omega^2 \boldsymbol{g} \cdot \overline{\boldsymbol{v}}\big) \boldsymbol{I}$$

$$\mathfrak{S}_0^N = -\mathrm{Re}\big(\rho_F \omega^2 D\boldsymbol{g}^\mathsf{T} \overline{\boldsymbol{v}}\big)$$

$$\mathfrak{S}_1 = -\mathrm{Re}\Big(\rho_F \omega^2 \big(((\boldsymbol{u} \cdot \boldsymbol{n}) \boldsymbol{I} - \boldsymbol{n} \otimes \boldsymbol{u}) \overline{q} + \big(\big(\overline{\boldsymbol{v}} \cdot \boldsymbol{n}\big) \boldsymbol{I} - \boldsymbol{n} \otimes \overline{\boldsymbol{v}}\big) p\big)\Big),$$

where $(p, \boldsymbol{u})$ solves the state equation (2.2) and $(q, \boldsymbol{v})$ the adjoint equation (4.14).

Proof. Expression (4.30) is obtained from (4.23). Using Lemma 4.5 and $\operatorname{div} \boldsymbol{\theta} = D\boldsymbol{\theta}$: $\boldsymbol{I}$, we compute

$$\begin{aligned} \boldsymbol{A}'(0) \nabla p \cdot \nabla \overline{q} &= \nabla p \cdot \nabla \overline{q} \operatorname{div} \boldsymbol{\theta} - D\boldsymbol{\theta} \nabla p \cdot \nabla \overline{q} - D\boldsymbol{\theta}^\mathsf{T} \nabla p \cdot \nabla \overline{q} \\ &= \nabla p \cdot \nabla \overline{q} (D\boldsymbol{\theta} : \boldsymbol{I}) - D\boldsymbol{\theta} : \Big(\nabla p \otimes \nabla \overline{q} + \nabla \overline{q} \otimes \nabla p\Big) \\ &= D\boldsymbol{\theta} : \Big(\Big(\nabla p \cdot \nabla \overline{q}\Big) \boldsymbol{I} - 2 \nabla p \odot \nabla \overline{q}\Big). \end{aligned}$$

Using $D_\Gamma \boldsymbol{\theta}^\mathsf{T} \boldsymbol{n} = D\boldsymbol{\theta}^\mathsf{T} \boldsymbol{n} - (D\boldsymbol{\theta} \boldsymbol{n} \otimes \boldsymbol{n})^\mathsf{T} \boldsymbol{n} = D\boldsymbol{\theta}^\mathsf{T} \boldsymbol{n} - (\operatorname{div} \boldsymbol{\theta}) \boldsymbol{n} + (\operatorname{div}_\Gamma \boldsymbol{\theta}) \boldsymbol{n}$ we get

$$\begin{aligned} (\boldsymbol{u} \cdot \boldsymbol{B}'(0) \boldsymbol{n}) \overline{q} &= \overline{q} \boldsymbol{u} \cdot \Big(\operatorname{div} \boldsymbol{\theta} \boldsymbol{n} - D\boldsymbol{\theta}^\mathsf{T} \boldsymbol{n}\Big) = \overline{q} \boldsymbol{u} \cdot \Big(- D_\Gamma \boldsymbol{\theta}^\mathsf{T} \boldsymbol{n} + (\operatorname{div}_\Gamma \boldsymbol{\theta}) \boldsymbol{n}\Big) \\ &= D_\Gamma \boldsymbol{\theta} : (- \boldsymbol{n} \otimes \boldsymbol{u} + (\boldsymbol{u} \cdot \boldsymbol{n}) \boldsymbol{I}) \overline{q}. \end{aligned}$$

Using Lemma 4.5, we have

$$\begin{aligned}\sigma'_{\boldsymbol{\theta}}(\boldsymbol{u}) : \varepsilon\left(\overline{\boldsymbol{v}}\right) &= \mu\left(D\boldsymbol{u}D\boldsymbol{\theta} + D\boldsymbol{\theta}^T D\boldsymbol{u}^T\right) : \varepsilon\left(\overline{\boldsymbol{v}}\right) + \lambda \text{ trace } \varepsilon'_{\boldsymbol{\theta}}(\boldsymbol{u})\boldsymbol{I} : \varepsilon\left(\overline{\boldsymbol{v}}\right) \\ &= \mu D\boldsymbol{\theta} : \left(D\boldsymbol{u}^{\mathsf{T}}\varepsilon\left(\overline{\boldsymbol{v}}\right) + D\boldsymbol{u}^{\mathsf{T}}\varepsilon\left(\overline{\boldsymbol{v}}\right)^{\mathsf{T}}\right) + \lambda(\boldsymbol{I} : \varepsilon'_{\boldsymbol{\theta}}(\boldsymbol{u}))\left(\boldsymbol{I} : \varepsilon\left(\overline{\boldsymbol{v}}\right)\right) \\ &= 2\mu D\boldsymbol{\theta} : D\boldsymbol{u}^{\mathsf{T}}\varepsilon\left(\overline{\boldsymbol{v}}\right) + \lambda(D\boldsymbol{\theta} : D\boldsymbol{u}^{\mathsf{T}})\left(\boldsymbol{I} : \varepsilon\left(\overline{\boldsymbol{v}}\right)\right) = D\boldsymbol{\theta} : D\boldsymbol{u}^{\mathsf{T}}\sigma\left(\overline{\boldsymbol{v}}\right)\end{aligned}$$

and

$$\begin{aligned}\sigma(\boldsymbol{u}) : \varepsilon'_{\boldsymbol{\theta}}\left(\overline{\boldsymbol{v}}\right) &= \sigma(\boldsymbol{u}) : \frac{1}{2}\left(D\overline{\boldsymbol{v}}D\boldsymbol{\theta} + D\boldsymbol{\theta}^T D\overline{\boldsymbol{v}}^T\right) = D\boldsymbol{\theta} : \frac{1}{2}\left(D\overline{\boldsymbol{v}}^{\mathsf{T}}\sigma(\boldsymbol{u}) + D\overline{\boldsymbol{v}}^{\mathsf{T}}\sigma(\boldsymbol{u})^{\mathsf{T}}\right) \\ &= D\boldsymbol{\theta} : D\overline{\boldsymbol{v}}^{\mathsf{T}}\sigma(\boldsymbol{u}).\end{aligned}$$

This yields (4.30).

The tensor form (4.30) is convenient for numerical implementation, and it allows to quickly compute the boundary expression of the shape derivative using (Laurain and Sturm, 2016, Proposition 4.3 and Corollary 4.5). Here we do not compute the boundary expression since we use the distributed expression (4.30) in the numerics.

In Theorem 4.10 and Proposition 4.11, we have computed the distributed shape derivative of J for a general class of shape perturbations $\Phi_t^{\boldsymbol{\theta}}$, which could, for instance, be applied to optimize the shape of the bead for noise reduction. In this paper, we are interested in a particular application where the shape of the bead is fixed and its position is optimized. For this application, Proposition 4.11 can be used with a class of rigid perturbations $\boldsymbol{\theta}$ described in Section 4.7.

4.7 Application to a bead optimization problem

In this section, we are going to apply the previous results to a problem of bead optimization. Beads or stampings are widely used to reduce vibration of structures without increasing their weight. A reduction of the vibration of a structure also reduces the sound level in the adjacent areas. Given a bead of a specific form, our aim is to find an optimal position of the bead on the plate of our model problem to reduce the sound level at a certain position for a fixed frequency ω. The plate of height $h \in \mathbb{R}, h > 0$ with the bead is described by the simply connected domain $\Sigma \subset \mathbb{R}^2$ and a bounded and Lipschitz continuous profile function $g : \Sigma \to \mathbb{R}$ in the following way:

$$\Omega_S := \left\{\boldsymbol{x} \in \mathbb{R}^3 : (x_1, x_2) \in \Sigma, g(x_1, x_2) - h < x_3 < g(x_1, x_2)\right\}.$$

The bead corresponds to the support of g, that is, the set where $g \neq 0$, while the region where $g = 0$ is flat. The fluid domain is considered above the plate

$$\Omega_F := \left\{\boldsymbol{x} \in \mathbb{R}^3 : (x_1, x_2) \in \Sigma, g(x_1, x_2) < x_3 < H(x_1, x_2)\right\}$$

with the bounded and Lipschitz continuous function $H : \Sigma \to \mathbb{R}$ satisfying $\inf_{(x_1,x_2)\in\Sigma} H(x_1, x_2) =: H_{\min} > g_{\max} := \sup_{(x_1,x_2)\in\Sigma} g(x_1, x_2)$. Then, the interface between the fluid and the solid structure is

$$\Gamma := \left\{\boldsymbol{x} \in \mathbb{R}^3 : (x_1, x_2) \in \Sigma, x_3 = g(x_1, x_2)\right\},$$

In Figure 2, a square plate with the bead also of square shape is illustrated in a top view. Here, g is a piecewise linear function.

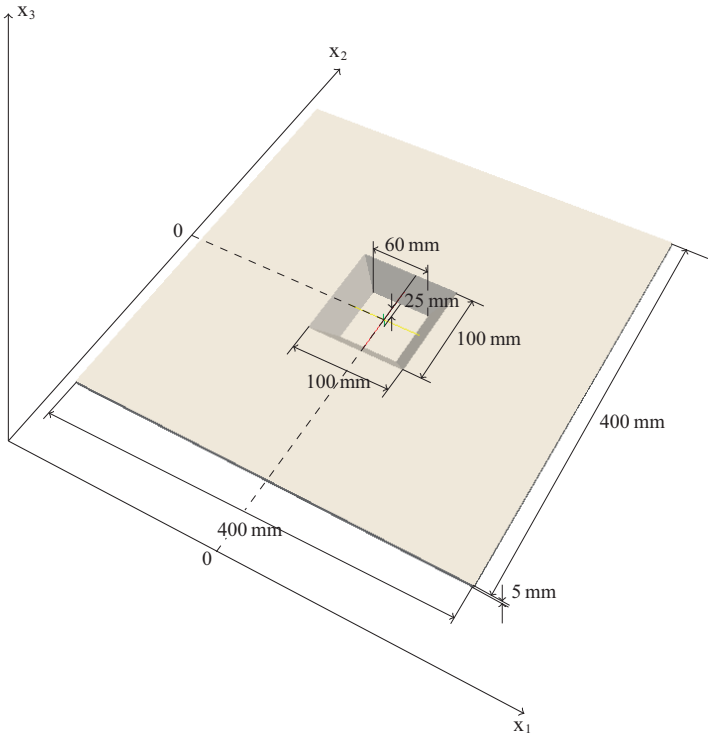

Figure 2.
Example of a square-shaped bead located at the center of a thin plate, used in numerical experiments

We only allow translations of the bead; therefore, we choose specific perturbations $\boldsymbol{\theta}$ accordingly. The position of the bead on the plate can be described by the position (d_1, d_2) of its center, whose components are used as the *design parameters*. Our aim is to formulate the shape derivative as a function of (d_1, d_2). We choose the perturbation $\boldsymbol{\theta} : \mathfrak{D} \to \mathbb{R}^3$ such that the corresponding transformation $\Phi_t^{\boldsymbol{\theta}}$ leaves a large part of Ω_S and Ω_F globally unchanged, and only a subdomain with and around the bead is translated. For this we use a continuous and piecewise smooth cutoff function $\eta : \mathfrak{D} \to \mathbb{R}$ that is equal to 1 in a ϵ-neighborhood of the bead and 0 outside a 2ϵ-neighborhood of the bead, where ϵ is chosen appropriately. Then, the translation of the bead is defined by

$$\boldsymbol{\theta} = \begin{pmatrix} \beta_1 \eta \\ \beta_2 \eta \\ 0 \end{pmatrix},$$

where $(\beta_1, \beta_2) \in \mathbb{R}^2$ represents a translation vector in the xy-plane; see Figure 3 for an illustration of $\boldsymbol{\theta}$ in the xy-plane.

Writing $\boldsymbol{\theta} = \beta_1 \boldsymbol{\theta}_1 + \beta_2 \boldsymbol{\theta}_2$ with

$$\boldsymbol{\theta}_1 = \begin{pmatrix} \eta \\ 0 \\ 0 \end{pmatrix} \quad \text{and} \quad \boldsymbol{\theta}_2 = \begin{pmatrix} 0 \\ \eta \\ 0 \end{pmatrix},$$

we introduce $\mathcal{J}(\beta_1, \beta_2) := J(\Phi_t^{\boldsymbol{\theta}}(\Omega_F), \Phi_t^{\boldsymbol{\theta}}(\Omega_S))$. Note that $\mathcal{J}(\beta_1, \beta_2)$ is a new function at each iteration since it depends on (Ω_F, Ω_S). Using the chain rule and Proposition 4.11, we have

$$\nabla \mathcal{J}(\beta_1, \beta_2) = \begin{pmatrix} dJ\left(\Omega_F, \Omega_S; \partial_{\beta_1}\boldsymbol{\theta}\right) \\ dJ\left(\Omega_F, \Omega_S; \partial_{\beta_2}\boldsymbol{\theta}\right) \end{pmatrix} = \begin{pmatrix} dJ(\Omega_F, \Omega_S; \boldsymbol{\theta}_1) \\ dJ(\Omega_F, \Omega_S; \boldsymbol{\theta}_2) \end{pmatrix} = \begin{pmatrix} h_1(\eta) \\ h_2(\eta) \end{pmatrix},$$

where, for $i = 1, 2$,

$$\begin{aligned} h_i(\eta) := dJ(\Omega_F, \Omega_S; \boldsymbol{\theta}_i) = &\int_{\Omega_F} \mathbf{S}_1^F : D\boldsymbol{\theta}_i + \mathbf{S}_0^F \cdot \boldsymbol{\theta}_i \, \mathrm{d}x + \int_{\Omega_S} \mathbf{S}_1^S : D\boldsymbol{\theta}_i + \mathbf{S}_0^S \cdot \boldsymbol{\theta}_i \, \mathrm{d}x \\ &+ \int_{\Gamma} \mathfrak{S}_1 : D_\Gamma \boldsymbol{\theta}_i \, \mathrm{d}\sigma + \int_{\Gamma_N} \mathfrak{S}_1^N : D_\Gamma \boldsymbol{\theta}_i + \mathfrak{S}_0^N \cdot \boldsymbol{\theta}_i . \, \mathrm{d}\sigma \end{aligned} \tag{4.31}$$

Choosing $(\beta_1, \beta_2) = -(h_1(\eta), h_2(\eta))$ we get

$$\begin{aligned} J\left(\Phi_t^{\boldsymbol{\theta}}(\Omega_F), \Phi_t^{\boldsymbol{\theta}}(\Omega_S)\right) &= J(\Omega_F, \Omega_S) + tdJ(\Omega_F, \Omega_S; \boldsymbol{\theta}) + O\left(t^2\right) \\ &= J(\Omega_F, \Omega_S) + t(\beta_1 h_1(\eta) + \beta_2 h_2(\eta)) + O\left(t^2\right) \\ &= J(\Omega_F, \Omega_S) - t(h_1(\eta)^2 + h_2(\eta)^2) + O\left(t^2\right). \end{aligned}$$

Thus, for sufficiently small t, $(\beta_1, \beta_2) = -(h_1(\eta), h_2(\eta))$ is a descent direction for $J(\Omega_F, \Omega_S)$. Then, starting from an initial bead position (d_1, d_2), we can update the position of the bead using

$$\begin{pmatrix} \widehat{d}_1 \\ \widehat{d}_2 \end{pmatrix} = \begin{pmatrix} d_1 \\ d_2 \end{pmatrix} + \alpha \begin{pmatrix} \beta_1 \\ \beta_2 \end{pmatrix},$$

where $\alpha > 0$ is determined by a line search.

4.8 Numerical results for a bead optimization problem

In this section, we present and interpret the results of the optimization for a square bead of 100 mm × 100 mm and a depth of 25 mm on a square plate of 400 mm × 400 mm and of 5 mm thickness. The fluid domain Ω_F is located above the plate and has constant height $H = 1{,}500$ mm. The bead has a depth of 25 mm in a centered square of 60 mm × 60 mm and its side flanks have trapezoidal shape. This means that the function g is linear on each of the four side flanks and its gradient is a normal vector of the nearest side of the 100 mm × 100 mm. On the lateral faces of the plate, we impose Dirichlet boundary conditions, and we apply the force $\boldsymbol{g} = (0,0,1)^T$ on the bottom face Γ_N; see Figure 1. On the lateral sides and the top face of the fluid part Ω_F, we impose homogeneous Neumann boundary conditions, and the force in the fluid is zero, that is, $\boldsymbol{f} = 0$.

We use the following material parameters: $c = 343 \cdot 10^3$ mm/s for the speed of sound in the air and $\lambda = 23{,}829$ N/mm^2, $\mu = 30{,}327$ N/mm^2 and $\rho_S = 0.25 \cdot 10^{-8}$ Ns^2/mm^4 for the structure parameters. We also take $\rho_F = 1.2041 \cdot 10^{-12}$ Ns^2/mm^4 = 1.2041 kg/m^3, which corresponds to the density of air at 20 °C.

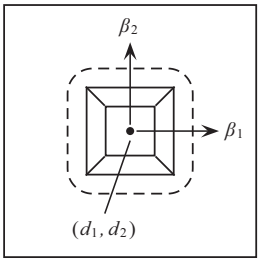

Figure 3.
Translation of the bead centered at (d_1, d_2). The perturbation $\boldsymbol{\theta} = (\beta_1\eta, \beta_2\eta, 0)^\top$ where η is a cut-off function, is constant within the dashed area

As already explained before, we limit ourselves to optimizing at a single frequency and not a frequency range. All of the following calculations were performed with the frequency 275 Hz. The first natural frequency of a flat plate, that is, a plate without bead, with the same dimensions, same material parameter and same but homogeneous boundary conditions as described above and in addition with traction free boundary condition on Γ is about 288 Hz. This frequency for the optimization is chosen considering that the influence of the first natural frequency of the flat plate is quite high. By placing the bead somewhere on the plate, we expect a stiffening of the structure and that the natural frequencies of the structure will be shifted to the right. We also expect that, by optimizing the position of the bead at this frequency, one can also measure a significant difference in sound pressure. As objective functional we choose

$$J(\Omega) := \int_B |p|^2 \, \mathrm{d}x,$$

where B is the ball of radius 50 mm and center (200 mm, 200 mm, 1,100 mm), that is, it is located 1,050 mm above the flat plate. The functional corresponds to (4.11) with $p_d = 0$ and a discontinuous function κ that is equal to 1 inside and equal to 0 outside the ball B. In (4.11) we have assumed $\kappa \in C^\infty(\mathfrak{D})$ to simplify the presentation, but the result can be extended to the case where κ is discontinuous as long as the discontinuity does not intersect the support of $\boldsymbol{\theta}$, which is the case here.

For the parameterized geometry of the plate with bead and the fluid domain above, we use Gmsh (Geuziane and Remacle, 2009) to automatically generate a hexahedral mesh. We use concepts (Frauenfelder and Lage, 2002) for a finite element discretization of the shape optimization problem of high order, where discrete trace spaces (Schmidt, 2008) are utilized for the coupling terms. For the numerical experiments, we use a mesh width of 50 mm, where the plate is resolved by one layer of thin elements. We use finite elements of polynomial degree 3 in the solid part and of polynomial degree 1 in the fluid part. We use the direct solver Mumps (Amestoy *et al.*, 2000) for solving the linear systems. In each step of the optimization problem the direction (β_1, β_2) is computed and the step size α is obtained via the SciPy standard line search (Virtanen *et al.*, 2020), where we use $\alpha < 0.05$ as stopping criterion.

The optimization in this numerical experiment was performed with different starting positions for the bead. In the following, the starting positions are described by local (x, y)-coordinates on the plate. In Figure 4, the sequences of positions of the bead and the associated

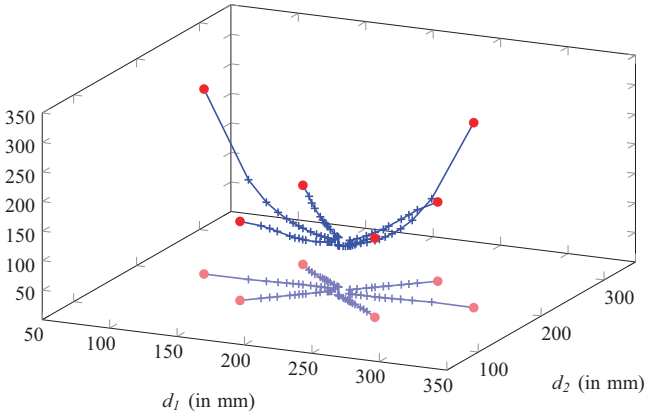

Figure 4.
Evolution of the bead position in the plane and of the associated objective function values during the optimization process, for various starting positions of the bead (red circles)

objective function values during the optimization process are shown, for six different starting positions (100 mm, 200 mm), (150 mm, 150 mm), (250 mm, 150 mm), (300 mm, 200 mm), (250 mm, 250 mm) and (150 mm, 250 mm). We observe that the iterates are converging toward the optimal position (200 mm, 200 mm) and the objective function clearly has a local minimum at this point. In all cases, the stopping criterion breaks the iteration about 5 mm before reaching the center position. For the starting position (100 mm, 200 mm), the optimized bead position reached in 14 iterations is (195.75 mm, 203.38 mm) and for the starting position (150 mm, 150 mm) the optimized position reached in 15 iterations is (196.01 mm, 197.31 mm). In Figure 5, these starting and optimized positions of the beads are shown.

In Figure 6(a), the distance of the bead position to the optimal center position is plotted as a function of the iteration number. We observe a linear convergence with an error reduction of about 17% per iteration step. The numerical error of the finite element solution as well as the numerical integration error in the calculation of the objective function or the shape derivative limits the achievable accuracy of the optimized position, which is, however, not visible at this

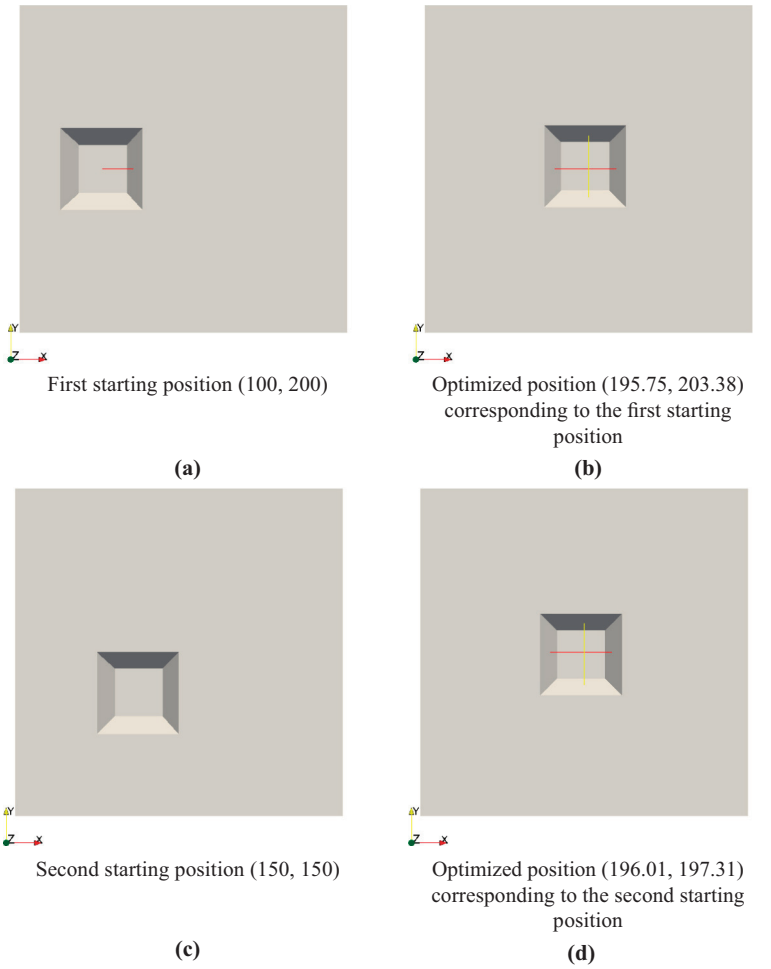

Figure 5.
Comparison of starting position and optimized position of the bead for the starting positions (100, 200) and (150, 150)

error level. In Figure 6(b), the objective function is plotted against the iteration number for the starting positions (100 mm, 200 mm) and (150 mm, 150 mm). It can be seen here that the objective function values hardly change in the last iteration steps. This justifies the choice of the stopping criterion as in practice there is only a very small difference whether the bead is exactly in the middle of the plate or is placed a few millimeters away from it, and further computations would not yield a significant improvement.

The optimization of only one frequency can bring improvements for the selected frequency, but may also result in deteriorations for other frequencies. In order to verify that the first natural frequency of the structure is shifted to the right, as well as to assess the possibly adverse effects on other frequencies, we compare the frequency responses to the starting positions and the optimized positions. In Figure 7, the frequency response for the plate without bead is compared to the frequency response with the bead at the first starting position and at the optimized bead position.

It can be seen that the bead at the starting position already causes an increase in rigidity and results in a shift to the right of the first natural frequency of the structure. The optimization reinforces this behavior and pushes the natural frequency further to the right. For the optimization, we used the frequency 275 Hz (dashed line in Figure 7). We observe an important reduction of the sound pressure in the frequency range around 275 Hz, which is due

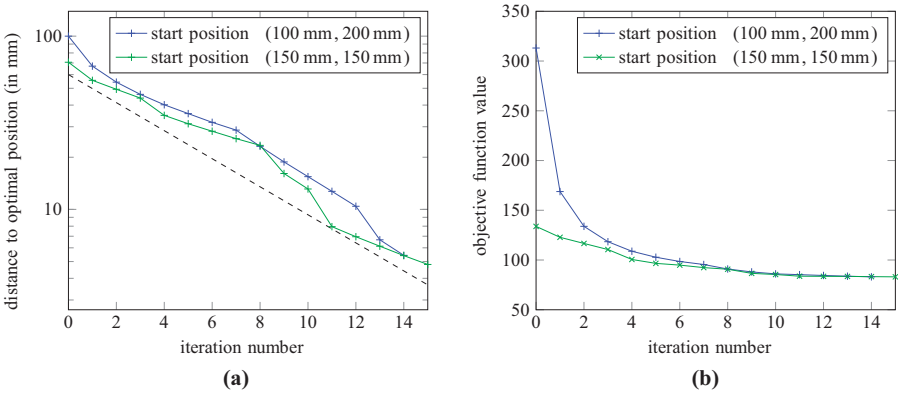

Figure 6.
(a) Distance to the optimal position (200 mm, 200 mm) and (b) objective function value plotted against the iteration number for the starting positions (100 mm, 200 mm) and (150 mm, 150 mm). The dashed line in (a) corresponds to reduction of the distance to the optimal position by 17% in each step

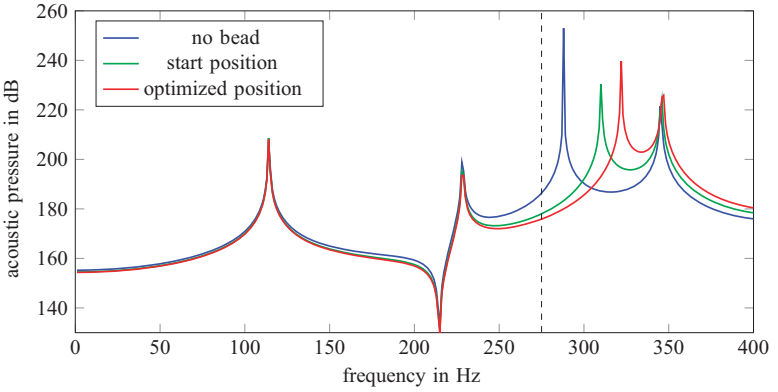

Figure 7.
Comparison of the frequency responses at the position (200 mm, 200, mm, 1,100 mm) for the plate without bead (blue), with a bead at starting position (100 mm, 200 mm) (green) and with a bead at the obtained optimal position (195.75 mm, 203.38 mm) for frequency 275 Hz (red)

to the proximity of the first eigenfrequency of the plate without bead at 288 Hz. Also, at lower frequencies and even at the beginning of the frequency response at 1 Hz, the sound pressure for the optimized bead position is lower than for the plate without bead. Thus, the optimization results in the reduction of the influence of the structural mode for the lower frequencies. However, we also observe that the sound pressure in the area after the original first natural frequency of the structure is now higher. This may be seen as an undesirable side effect of optimizing only for one frequency, for which a possible remedy would be to simultaneously optimize for several different frequencies.

References

Akl, W., El-Sabbagh, A., Al-Mitani, K. and Baz, A. (2009), "Topology optimization of a plate coupled with acoustic cavity", *International Journal of Solids and Structures*, Vol. 46 No. 10, pp. 2060-2074, Special Issue in Honor of Professor Liviu Librescu.

Allaire, G., Jouve, F. and Toader, A.-M. (2004), "Structural optimization using sensitivity analysis and a level-set method", *Journal of Computational Physics*, Vol. 194 No. 1, pp. 363-393.

Allaire, G., Dapogny, C., Delgado, G. and Michailidis, G. (2014), "Multi-phase structural optimization *via* a level set method", *ESAIM. Control, Optimisation and Calculus of Variations*, Vol. 20 No. 2, pp. 576-611.

Amestoy, P.R., Duff, I.S., L'Excellent, J.-Y. and Koster, J. (2000), "Mumps: a general purpose distributed memory sparse solver", *International Workshop on Applied Parallel Computing*, Springer, pp. 121-130.

Antil, H., Hardesty, S. and Heinkenschloss, M. (2017), "Shape optimization of shell structure acoustics", *SIAM Journal on Control and Optimization*, Vol. 55 No. 3, pp. 1347-1376.

Barucq, H., Djellouli, R. and Estecahandy, E. (2014), "On the existence and the uniqueness of the solution of a fluid-structure interaction scattering problem", *Journal of Mathematical Analysis and Applications*, Vol. 412 No. 2, pp. 571-588.

Beretta, E., Francini, E. and Vessella, S. (2017), "Differentiability of the Dirichlet to Neumann map under movements of polygonal inclusions with an application to shape optimization", *SIAM Journal on Mathematical Analysis*, Vol. 49 No. 2, pp. 756-776.

Berggren, M. (2010), "A unified discrete-continuous sensitivity analysis method for shape optimization", *Applied and Numerical Partial Differential Equations, Vol. 15, of Comput. Methods Appl. Sci.*, Springer, New York, pp. 25-39.

Céa, J. (1986), "Conception optimale ou identification de formes: calcul rapide de la dérivée directionnelle de la fonction coût", *RAIRO Modélisation Mathématique et Analyse Numérique*, Vol. 20 No. 3, pp. 371-402.

Ciarlet, P.G. (1988), "Mathematical elasticity: Volume I: three dimensional elasticity", *Studies in Mathematics and its Applications*, North-Holland Publishing, Amsterdam, Vol. 20, p. xlii+451, ISBN 0-444-70259-8.

Delfour, M. (2012), "Introduction to optimization and semidifferential calculus", in *MOS-SIAM Series on Optimization*, Society for Industrial and Applied Mathematics (SIAM), Mathematical Optimization Society, Philadelphia, PA, Vol. 12, p. xvi+353, ISBN 978-1-611972-14-6, doi: 10.1137/1.9781611972153.

Delfour, M.C. and Zolésio, J.-P. (1988a), "Shape sensitivity analysis via a penalization method", *Annali di Matematica Pura ed Applicata*, Serie Quarta, Vol. 151, pp. 179-212.

Delfour, M.C. and Zolésio, J.-P. (1988b), "Shape sensitivity analysis via min max differentiability", *SIAM Journal on Control and Optimization*, Vol. 26 No. 4, pp. 834-862.

Delfour, M.C. and Zolésio, J.-P. (2011), *Shapes and Geometries: MetrAics, Analysis, Differential Calculus, and Optimization, Vol. 22, of Advances in Design and Control*, 2nd ed., Society for Industrial and Applied Mathematics (SIAM), Philadelphia, PA.

Delfour, M., Payre, G. and Zolésio, J.-P. (1985), "An optimal triangulation for second-order elliptic problems", *Computer Methods in Applied Mechanics and Engineering*, Vol. 50 No. 3, pp. 231-261.

Delfour, M.C., Mghazli, Z. and Zolésio, J.-P. (1997), "Computation of shape gradients for mixed finite element formulation", *Partial Differential Equation Methods in Control and Shape Analysis (Pisa), Vol. 188, of Lecture Notes in Pure and Applied Mathematics*, Dekker, New York, pp. 77-93.

Dilgen, C.B., Dilgen, S.B., Aage, N. and Jensen, J.S. (2019), "Topology optimization of acoustic mechanical interaction problems: a comparative review", *Structural and Multidisciplinary Optimization*, Vol. 60 No. 2, pp. 779-801.

Du, J. and Olhoff, N. (2007), "Minimization of sound radiation from vibrating bi-material structures using topology optimization", *Structural and Multidisciplinary Optimization*, Vol. 33 Nos 4-5, pp. 305-321.

Du, J. and Olhoff, N. (2010), "Topological design of vibrating structures with respect to optimum sound pressure characteristics in a surrounding acoustic medium", *Structural and Multidisciplinary Optimization*, Vol. 42 No. 1, pp. 43-54.

Eigel, M. and Sturm, K. (2018), "Reproducing kernel Hilbert spaces and variable metric algorithms in PDE-constrained shape optimization", *Optimization Methods and Software*, Vol. 33 No. 2, pp. 268-296.

Eshelby, J.D. (1975), "The elastic energy-momentum tensor", *Journal of Elasticity: The Physical and Mathematical Science of Solids*, Vol. 5 Nos 3-4, pp. 321-335, Special Issue Dedicated to A.E. Green.

Etling, T. and Herzog, R. (2018), "Optimum experimental design by shape optimization of specimens in linear elasticity", *SIAM Journal on Applied Mathematics*, Vol. 78 No. 3, pp. 1553-1576.

Evans, L.C. (2010), "Partial differential equations", in Graduate Studies in Mathematics, 2nd ed., American Mathematical Society, Providence, RI, Vol. 19, p. xxii+749, ISBN 978-0-8218-4974-3, doi: 10.1090/gsm/019.

Frauenfelder, P. and Lage, C. (2002), "Concepts – an object-oriented software package for partial differential equations", *Mathematical Modelling and Numerical Analysis*, Vol. 36 No. 5, pp. 937-951.

Fulmański, P., Laurain, A., Scheid, J.-F. and Sokołowski, J. (2007), "A level set method in shape and topology optimization for variational inequalities", *International Journal of Applied Mathematics and Computer Science*, Vol. 17 No. 3, pp. 413-430.

Fulmański, P., Laurain, A., Scheid, J.-F. and Sokołowski, J. (2008), "Level set method with topological derivatives in shape optimization", *International Journal of Computer Mathematics*, Vol. 85 No. 10, pp. 1491-1514.

Gangl, P., Langer, U., Laurain, A., Meftahi, H. and Sturm, K. (2015), "Shape optimization of an electric motor subject to nonlinear magnetostatics", *SIAM Journal on Scientific Computing*, Vol. 37 No. 6, pp. B1002-B1025.

Geuziane, C. and Remacle, J.-F. (2009), "Gmsh: a three-dimensional finite element mesh generator with built-in pre- and post-processing facilities", *International Journal for Numerical Methods in Engineering*, Vol. 79 No. 11, pp. 1309-1331.

Giacomini, M., Pantz, O. and Trabelsi, K. (2017), "Certified descent algorithm for shape optimization driven by fully-computable *a posteriori* error estimators", *ESAIM. Control, Optimisation and Calculus of Variations*, Vol. 23 No. 3, pp. 977-1001.

Henrot, A. and Pierre, M. (2018), *Shape Variation and Optimization. A Geometrical Analysis, Vol. 28, of EMS Tracts in Mathematics*, European Mathematical Society (EMS), Zürich, English Version of the French Publication [MR2512810] with Additions and Updates.

Hintermüller, M. and Laurain, A. (2009), "Multiphase image segmentation and modulation recovery based on shape and topological sensitivity", *Journal of Mathematical Imaging and Vision*, Vol. 35 No. 1, pp. 1-22.

Hintermüller, M., Laurain, A. and Yousept, I. (2015), "Shape sensitivities for an inverse problem in magnetic induction tomography based on the eddy current model", *Inverse Problems*, Vol. 31 No. 6, p. 25, 065006.

Hiptmair, R., Paganini, A. and Sargheini, S. (2015), "Comparison of approximate shape gradients", *BIT. Numerical Mathematics*, Vol. 55 No. 2, pp. 459-485.

Ito, K., Kunisch, K. and Peichl, G.H. (2008), "Variational approach to shape derivatives", *ESAIM. Control, Optimisation and Calculus of Variations*, Vol. 14 No. 3, pp. 517-539.

Kasumba, H. and Kunisch, K. (2011), "On shape sensitivity analysis of the cost functional without shape sensitivity of the state variable", *Control and Cybernetics*, Vol. 40 No. 4, pp. 989-1017.

Kasumba, H. and Kunisch, K. (2014), "On computation of the shape hessian of the cost functional without shape sensitivity of the state variable", *Journal of Optimization Theory and Applications*, Vol. 162 No. 3, pp. 779-804, doi: 10.1007/s10957-013-0520-4.

Kato, T. (1995), *Perturbation theory for linear operators, Grundlehren der mathematischen Wissenschaften*, Springer, Berlin and Heidelberg.

Laurain, A. (2018), "A level set-based structural optimization code using FEniCS", *Structural and Multidisciplinary Optimization*, Vol. 58 No. 3, pp. 1311-1334.

Laurain, A. (2020), "Distributed and boundary expressions of first and second order shape derivatives in nonsmooth domains", *Journal de Mathématiques Pures et Appliquées*, Vol. 134, pp. 328-368.

Laurain, A. and Sturm, K. (2016), "Distributed shape derivative *via* averaged adjoint method and applications", *ESAIM. Mathematical Modelling and Numerical Analysis*, Vol. 50 No. 4, pp. 1241-1267.

Laurain, A., Lopes, P.T.P. and Nakasato, J.C. (2020), "An abstract lagrangian framework for computing shape derivatives", arXiv:2011.00873v1 [math.OC].

Luo, J. and Gea, H.C. (2003), "Optimal stiffener design for interior sound reduction using a topology optimization based approach", *Journal of Vibration and Acoustics*, Vol. 125 No. 3, p. 267.

Marburg, S. (2002), "Developments in structural-acoustic optimization for passive noise control", *Archives of Computational Methods in Engineering*, Vol. 9 No. 4, pp. 291-370.

Marburg, S., Shepherd, M. and Hambric, S.A. (2016), "Structural-acoustic optimization", *Engineering Vibroacoustic Analysis*, John Wiley & Sons, pp. 268-304.

McLean, W. (2000), *Strongly Elliptic Systems and Boundary Integral Equations*, Cambridge Univarsity Press, Cambridge, p. xiv+357, ISBN 0-521-66332-6; 0-521-66375-X.

Novotny, A.A. and Sokołowski, J. (2013), "Topological derivatives in shape optimization", *Interaction of Mechanics and Mathematics*, Springer, Heidelberg.

Osher, S. and Sethian, J.A. (1988), "Fronts propagating with curvature-dependent speed: algorithms based on Hamilton-Jacobi formulations", *Journal of Computational Physics*, Vol. 79 No. 1, pp. 12-49.

Pantz, O. (2005), "Sensibilité de l'équation de la chaleur aux sauts de conductivité", *Comptes Rendus Mathématique*, Vol. 341, Académie des Sciences, Paris, No. 5, pp. 333-337.

Sauter, S. and Schwab, C. (2011), *Boundary Element Methods*, Springer, Berlin and Heidelberg.

Schmidt, K. (2008), "High-order numerical modelling of highly conductive thin sheets", PhD Thesis, ETH Zurich.

Schmidt, S. (2018), "Weak and strong form shape Hessians and their automatic generation", *SIAM Journal on Scientific Computing*, Vol. 40 No. 2, pp. C210-C233.

Schulz, V.H., Siebenborn, M. and Welker, K. (2016), "Efficient PDE constrained shape optimization based on Steklov-Poincaré-type metrics", *SIAM Journal on Optimization*, Vol. 26 No. 4, pp. 2800-2819.

Shu, L., Wang, M.Y. and Ma, Z. (2014), "Level set based topology optimization of vibrating structures for coupled acoustic–structural dynamics", *Computers and Structures*, Vol. 132, pp. 34-42.

Sokolowski, J. and Zolesio, J.-P. (1992), *Introduction to Shape Optimization: Shape Sensitivity Analysis, Vol. 16, of Springer Series in Computational Mathematics*, Springer.

Stammberger, M. and Voss, H. (2014), "Variational characterization of eigenvalues of a non-symmetric eigenvalue problem governing elastoacoustic vibrations", *Applications of Mathematics*, Vol. 59 No. 1, pp. 1-13.

Sturm, K. (2015), "Minimax Lagrangian approach to the differentiability of nonlinear PDE constrained shape functions without saddle point assumption", *SIAM Journal on Control and Optimization*, Vol. 53 No. 4, pp. 2017-2039.

Sturm, K., Hintermüller, M. and Hömberg, D. (2016), "Distortion compensation as a shape optimisation problem for a sharp interface model", *Computational Optimization and Applications. An International Journal*, Vol. 64 No. 2, pp. 557-588.

van Dijk, N.P., Maute, K., Langelaar, M. and van Keulen, F. (2013), "Level-set methods for structural topology optimization: a review", *Structural and Multidisciplinary Optimization*, Vol. 48 No. 3, pp. 437-472.

Vicente, W., Picelli, R., Pavanello, R. and Xie, Y. (2015), "Topology optimization of frequency responses of fluid–structure interaction systems", *Finite Elements in Analysis and Design*, Vol. 98, pp. 1-13.

Virtanen, P., Gommers, R., Oliphant, T.E., Haberland, M., Reddy, T., Cournapeau, D., Burovski, E., Peterson, P., Weckesser, W., Bright, J., van der Walt, S.J., Brett, M., Wilson, J., Millman, K.J., Mayorov, N. and others SciPy 1.0 Contributors (2020), "SciPy 1.0: fundamental algorithms for scientific computing in Python", *Nature Methods*, Vol. 17, pp. 261-272.

Wang, M.Y., Wang, X. and Guo, D. (2003), "A level set method for structural topology optimization", *Computer Methods in Applied Mechanics and Engineering*, Vol. 192 Nos 1-2, pp. 227-246.

Yoon, G.H., Jensen, J.S. and Sigmund, O. (2006), "Topology optimization for acoustic-structure interaction problems", in Bendsøe, M.P., Olhoff, N. and Sigmund, O. (Eds), *IUTAM Symposium on Topological Design Optimization of Structures, Machines and Materials, Vol. 137, of Solid Mechanics and Its Applications*, Springer, pp. 355-364.

Yoon, G.H., Jensen, J.S. and Sigmund, O. (2007), "Topology optimization of acoustic-structure interaction problems using a mixed finite element formulation", *International Journal for Numerical Methods in Engineering*, Vol. 70 No. 9, pp. 1049-1075.

Corresponding author
Antoine Laurain can be contacted at: laurain@ime.usp.br